CHAPTER 9

Blending of Miscible Liquids

RICHARD K. GRENVILLE

The DuPont Company

ALVIN W. NIENOW

University of Birmingham

9-1 INTRODUCTION

Blending is a common mixing operation in the chemical and process industries. The objective is to take two or more miscible fluids and blend them to a predetermined degree of homogeneity. The time taken to reach this degree of homogeneity is the *blend time*. This is also known as the *macroscale mixing time* since it is the time scale associated with mixing the contents of a vessel.

Blending operations are carried out for low viscosity fluids in the turbulent regime, moderately viscous fluids in the transitional regime, and highly viscous fluids in the laminar regime. In most cases, the viscous fluids will be non-Newtonian and generally shear thinning. This must be taken into account in the design of appropriate mixing equipment. Occasionally, the fluids may exhibit a yield stress and/or viscoelasticity, and these complex behaviors also need to be considered, although viscoelasticity is not going to be considered here (see Section 4-2.2.1).

Agitated and jet mixed vessels are used for blending duties. The choice of equipment will depend on the viscosity of the fluid, the desired blend time, and the size of the vessel. The chapter is divided into four sections that cover design rules for:

- Blending of Newtonian fluids in the turbulent and transitional regimes (Re > 200) for turbine and hydrofoil impellers

Handbook of Industrial Mixing: Science and Practice, Edited by Edward L. Paul, Victor A. Atiemo-Obeng, and Suzanne M. Kresta
ISBN 0-471-26919-0

- Blending of shear-thinning fluids in the turbulent and transitional regimes (Re > 200) for turbine and hydrofoil impellers
- Agitation of yield stress fluids
- Blending of Newtonian and shear-thinning fluids in the laminar regime with helical ribbon impellers
- Jet mixing of low viscosity fluids in the turbulent regime

9-2 BLENDING OF NEWTONIAN FLUIDS IN THE TURBULENT AND TRANSITIONAL REGIMES

9-2.1 Literature Survey

Blend times have been measured in agitated vessels using a variety of techniques; conductivity, temperature, or pH (using an indicator for color change, as discussed in Section 4-4 and illustrated on the Visual Mixing CD). The results are presented as a relationship between the dimensionless blend time, which is the product of the measured blend time and the impeller rotational speed, dimensionless geometrical ratios, and in some cases, Reynolds and Froude numbers.

9-2.1.1 Turbulent Regime. The majority of references in the literature report that in the turbulent regime, the dimensionless blend time is a constant, independent of Reynolds and Froude numbers. The value of the constant is dependent on the impeller type and diameter relative to the vessel. These references include Kramers et al. (1953), Procházka and Landau (1961), Hoogendoorn and den Hartog (1967), Khang and Levenspiel (1976), Sano and Usui (1987), and others. There is a smaller group of references that report a weak dependence on Reynolds and Froude numbers in the turbulent regimes, and these include Fox and Gex (1956) and Norwood and Metzner (1960).

9-2.2 Development of the Design Correlation

The recommended correlations for design of agitators for blending in the turbulent and transitional regimes were developed at the Fluid Mixing Processes consortium at Cranfield in the U.K. The work is discussed in detail in Grenville (1992). Briefly, blend times were measured using a conductivity technique in vessels 0.30, 0.61, 1.83, and 2.97 m in diameter. The vessels had a standard torispherical base and were all fitted with standard baffles. The correlation is based on experiments carried out with one impeller located one-third of the liquid depth above the vessel base.

A variety of impellers were tested, including hydrofoils, pitched and flat blade turbines, and disk turbines, and their diameters ranged from one-third to one-half of the vessel diameter. Three conductivity probes were placed in the vessel in regions of differing agitation intensity (see Chapter 4):

- *Beneath the impeller:* T/50 below the impeller, T/8 from the shaft axis

- *Halfway between the agitator shaft and the vessel wall:* T/4.5 below the liquid surface, T/4.7 from the shaft axis
- *Behind a baffle:* T/3 below the liquid surface, T/2.2 from the shaft axis

In the turbulent regime, the local blend times were the same. In the transitional regime, the blend time measured beneath the impeller did not change significantly, but behind the baffle, the blend time increased. Ultimately, the local blend time behind the baffle controlled the blend time for the entire vessel.

9-2.2.1 Turbulent Regime. After rounding off the exponents obtained from regression of the data, the correlation for blend time to reach 95% homogeneity for all the impellers at all the scales tested by Grenville (1992) is

$$Po^{1/3} N\theta_{95} \frac{D^2}{T^{1.5} H^{0.5}} = 5.20 \tag{9-1}$$

The standard deviation of the constant is ±10.0%.

In a vessel where the liquid depth is equal to the vessel diameter,

$$Po^{1/3} N\theta_{95} \left(\frac{D}{T}\right)^2 = 5.20 \tag{9-2}$$

Since the impeller's power number is constant in a baffled vessel operating in the turbulent regime, $N\theta$ is a constant and independent of Reynolds number.

The equation can be rearranged to

$$Po^{1/3} ND^2 = 5.20 \frac{T^2}{\theta_{95}} \tag{9-3}$$

Multiplying both sides by ρ/μ yields

$$Po^{1/3} \frac{\rho ND^2}{\mu} = 5.20 \frac{\rho T^2}{\mu \theta_{95}} \tag{9-4}$$

$$Po^{1/3} Re = \frac{5.20}{Fo} \tag{9-5}$$

The dimensionless groups on the left-hand side are the power and Reynolds numbers of the impeller. The dimensionless group on the right-hand side is the Fourier number that is used in analysis of unsteady transfer processes. Hoogendoorn and den Hartog (1967) used it in their work but called it the *vessel Reynolds number*.

In an area where many studies have been made leading to different correlations, it is very valuable if independent corroborating work is available. Nienow (1997) found that blend time data already published with his co-workers or available from them fitted eq. (9-2) very well. This additional work covered further impeller types and a wider range of energy dissipation rates (down to 0.01 W/kg

found in fermenters containing animal cell cultures), although still in the turbulent regime. He also gave some theoretical justification for the relationships based on fundamental turbulence concepts from Corrsin (1964). The critical assumptions in the analysis were that the macro scale of turbulence was related to the diameter of the vessel, and the critical local energy dissipation rate was that at the wall.

9-2.2.2 Transitional Regime. The data taken in the transitional regime were correlated by performing a regression of $Po^{1/3}Re$ on $1/Fo$:

$$Po^{1/3}Re = \frac{183}{\sqrt{Fo}} \tag{9-6}$$

The standard deviation on the constant is $\pm 17.4\%$. This equation can be expanded to give

$$N\theta_{95} = \frac{183^2}{Po^{2/3}Re}\left(\frac{T}{D}\right)^2 \tag{9-7}$$

Since the power number is roughly constant in the transitional regime (the variation with Re is much less than the 1/Re dependence observed in the laminar regime), the dimensionless blend time is inversely proportional to Reynolds number, as other workers found.

Solving the two correlations for $Po^{1/3}Re$ on $1/Fo$ gives the values of these two dimensionless groups at the boundary between the turbulent and transitional regimes:

$$Po^{1/3}Re_{TT} = 6370 \qquad \text{and} \qquad \frac{1}{Fo_{TT}} = 1225$$

9-2.3 Use of the Design Correlation

There are two ways in which an engineer may have to use the blend time correlation; the first is to design a new agitator, and the second is to rate an existing agitator for a new process. Expressing the correlation in terms of $Po^{1/3}Re$ and $1/Fo$ makes this easier to do. When designing a new process, the vessel size, fluid physical properties, and desired blend time will be specified and $1/Fo$ can be calculated. Immediately, the regime in which the impeller will operate can be identified. The appropriate correlation can be used to calculate $Po^{1/3}Re$. The impeller type and diameter must be chosen such that so that the rotational speed necessary to achieve the desired blend time can be calculated.

When rating an existing agitator/vessel, the impeller type, speed, and diameter are known with the fluid physical properties. Now $Po^{1/3}Re$ can be calculated and the operating regime identified. Then $1/Fo$ can be calculated and the blend time calculated as the final step. Also, the standard deviation of the constants can be used to give a level of confidence to be included in the design procedure.

Approximately 67% of observations will lie within ±1 standard deviation. Similarly, 95% lie within ±2 standard deviations and 99% lie within ±3 standard deviations. So the level of confidence can be incorporated into the design process by defining the correlation constant to be used as:

turbulent regime: $5.20 + 0.52s$

transitional regime: $183 + 31.1s$

where s = 1 for 67% confidence level, s = 2 for 95% confidence level, and s = 3 for 99% confidence level. Examples of the correlation's use are given at the end of this section.

9-2.4 Impeller Efficiency

The question of which impeller is the most efficient for blending can be answered by rearranging the blend time correlations. In the turbulent regime, for a vessel where H = T,

$$Po^{1/3} N\theta_{95} \left(\frac{D}{T}\right)^2 = 5.20 \tag{9-2}$$

$$\theta_{95} \propto \left(\frac{T^3}{Po \cdot N^3 D^5}\right)^{1/3} \left(\frac{T}{D}\right)^{1/3} T^{2/3} \tag{9-8}$$

$$\theta_{95} \propto \left(\frac{1}{\bar{\varepsilon}}\right)^{1/3} \left(\frac{T}{D}\right)^{1/3} T^{2/3} \tag{9-9}$$

This analysis shows that:

- All impellers of the same diameter are equally energy efficient (i.e., achieve the same blend time at the same power per unit mass of fluid, $\bar{\varepsilon}$).
- A larger impeller diameter will achieve a shorter blend time for the same power input per unit mass.
- Blend time is independent of the fluid's physical properties in the turbulent regime.
- When scaling-up at constant power per unit mass and geometry, blend time will increase by the scale factor raised to the two-thirds power.

These conclusions are strongly supported by the theoretical analysis and experimental results of Nienow (1997) and Langheinrich et al. (1998). Most surprising is the conclusion concerning the equivalence of different impellers, which is counter-intuitive and contrary to what many vendors claim.

A similar analysis for the transitional regime leads to some similar conclusions but some which are quite different:

$$N\theta_{95} = \frac{183^2}{Po^{2/3}Re}\left(\frac{T}{D}\right)^2 \tag{9-7}$$

$$\theta_{95} \propto \left(\frac{T^3}{Po \cdot N^3 D^5}\right)^{2/3}\left(\frac{\mu}{\rho}\right) D^{-2/3} \tag{9-10}$$

$$\theta_{95} \propto \left(\frac{T^3}{Po \cdot N^3 D^5}\right)^{2/3}\left(\frac{\mu}{\rho}\right)\left(\frac{T}{D}\right)^{2/3} T^{-2/3} \tag{9-11}$$

$$\theta_{95} \propto \left(\frac{1}{\bar{\varepsilon}}\right)^{2/3}\left(\frac{\mu}{\rho}\right)\left(\frac{T}{D}\right)^{2/3} T^{-2/3} \tag{9-12}$$

This analysis shows that:

- All impellers of the same diameter are equally energy efficient (i.e., achieve the same blend time at the same power per unit mass of fluid, $\bar{\varepsilon}$).
- A larger impeller diameter will achieve a shorter blend time for the same power input per unit mass.
- Blend time is proportional to the fluid viscosity and inversely proportional to the density.
- When scaling-up at constant power per unit mass and geometry, blend time will *decrease* by the scale factor raised to the two-thirds power.

The first two conclusions are the same as for turbulent operation, but the last two are different. The final one in particular, that blend time will decrease on scale-up, may seem odd. However, it is correct, and the reason for this is that scaling-up at constant power input per unit mass, the Reynolds number will increase and the dimensionless blend time is inversely proportional to Reynolds number. This shows that care needs to be taken when scaling-up from lab or pilot scale vessels, which may be operating in the transitional regime, to plant scale, which may be operating in the turbulent regime. Using the design methods described above will take care of this scaling issue.

9-2.5 Shaft Torque, Critical Speed, and Retrofitting

Another consideration is the shaft torque. Since impellers of the same diameter require the same power input to achieve the same blend time, an impeller with a lower power number will have to operate at a higher speed and hence will have a lower shaft torque ($P = 2\pi N\Lambda$). Since the size of the shaft and gearbox are related to the torque, reducing the torque may reduce the agitator size and reduce the cost.

One factor to be aware of when making this decision is the critical speed of the shaft and impeller assembly. Running at a higher speed may reduce the torque, but the agitator may require a larger shaft anyway because the operating speed is

now too close to the first critical speed. On the other hand, a high-power-number agitator may be replaced by a lower Po agitator while the speed is maintained. If the diameter is increased so that the power and torque stay the same, critical speed problems are generally avoided, while the mixing time is shortened. This is a modestly effective retrofitting strategy.

9-2.6 Nonstandard Geometries: Aspect Ratios Greater Than 1 and Multiple Impellers

Cooke et al. (1988) reported mixing times for a range of multiple-impeller systems. They found the time increased very significantly but did not distinguish whether the increase was due particularly to the increase in height or the extra number of impellers. The equation that they gave for multiple Rushton turbines is similar to eq. (9-2):

$$\theta_m = \frac{3.3}{Po^{1/3}N}\left(\frac{H}{D}\right)^{2.43} \tag{9-13}$$

Cronin et al. (1994) showed by a decolorization technique the staged mixing associated with radial flow Rushton turbines, and Otomo et al. (1993) showed similar results with radial flow hollow-blade turbines. The latter also used conductivity probes and found mixing times about twice as long as with a single impeller, with values close to the predictions of the equation of Cooke et al. (1988).

When using two down-pumping wide-blade Lightnin A315 hydrofoil impellers in a vessel containing liquid with an aspect ratio of 2, Otomo et al. (1995) found that staged mixing or zoning was largely eliminated. As a result, the mixing time was significantly reduced compared to that of two radial flow impellers, typically by about 50% at the same specific energy dissipation rate. At the same aspect ratio, Hari-Prajitno et al. (1998) found a similar reduction with two up-pumping wide-blade hydrofoils (40%) and an even greater reduction with an up-pumping hydrofoil below a down-pumping (60%). The use of a radial flow impeller beneath either up-pumping (Vrabel et al., 2000) or down-pumping hydrofoils (Manikowski et al., 1994) is also quite effective as a means of lowering the mixing time and reducing zoning compared to radial flow impellers.

Clearly, once multiple impellers are employed, particularly with aspect ratios significantly different from 1, the system becomes considerably more complex. Mixing times can greatly increase and the choice of impellers now can be very significant.

9-2.7 Other Degrees of Homogeneity

The design correlation is based on experiments in which the blend time required to reach 95% homogeneity were measured. The blend time required to reach another degree of homogeneity can be calculated because the blending process is first order (i.e., the concentration fluctuations which are being "smoothed" as

the blending progresses decay exponentially):

$$\frac{dc'}{dt} = -kc' \tag{9-14}$$

$$\int_1^x \frac{dc'}{c'} = -k\int_0^\theta dt \tag{9-15}$$

$$[\ln c']_1^x = -k[t]_0^\theta \tag{9-16}$$

$$\ln(1 - x) = -k\theta \tag{9-17}$$

Here x is the relative magnitude of the concentration fluctuations and equals 1 at time $t = 0$ (i.e., 0% homogeneity). For 95% homogeneity, $x = 0.05$. So the equation to adjust the blend time for a degree of homogeneity other than 95% is

$$\theta_z = \theta_{95}\frac{\ln[(100 - \%\text{ homogeneity})/100]}{\ln 0.05} \tag{9-18}$$

If the blend time for 99% homogeneity is required,

$$\theta_{99} = \theta_{95}\frac{\ln[(100 - 99)/100]}{\ln 0.05} \tag{9-19}$$

$$\theta_{99} = \theta_{95}\frac{\ln 0.01}{\ln 0.05} = 1.537\theta_{95} \tag{9-20}$$

9-2.8 Examples

Example 9-1: Designing a New Agitator. A new process is to be carried out in a baffled vessel that is 6 ft (1.83 m) in diameter. The liquid depth will be 6 ft (1.83 m). At the end of the process an inhibitor is added to stop the reaction and it must be blended to 99.5% homogeneity within 0.5 min to prevent "overreaction" and production of a product with too high a molecular weight. At this point in the process the fluid has a specific gravity of 1.02 and a viscosity of 18 cP.

SOLUTION

1. Determine the operating regime by calculating 1/Fo. In SI units:

viscosity: $\mu = 0.018\ \text{Pa} \cdot \text{s}$

density: $\rho = 1020\ \text{kg/m}^3$

desired blend time: $\theta = 30\ \text{s}$

vessel diameter: $T = 1.83\ \text{m}$

$$\frac{1}{\text{Fo}} = \frac{\rho T^2}{\mu\theta} = \frac{1020\ \text{kg/m}^3 \times (1.83\ \text{m})^2}{0.018\ \text{Pa} \cdot \text{s} \times 30\ \text{s}} = 6326$$

The process will operate in the turbulent regime since $1/\text{Fo} > 1225$.

2. Determine the multiplier to convert 95% to 99.5% blend times:

$$\theta_{99.5} = \theta_{95}\frac{\ln[(100-99.5)/100]}{\ln 0.05}$$

$$\theta_{99} = \theta_{95}\frac{\ln 0.005}{\ln 0.05} = 1.768\theta_{95}$$

So the constant in the calculation will be 9.19 (i.e., 5.20×1.77).

3. Calculate $Po^{1/3}Re$ using the turbulent correlation with the adjusted constant:

$$Po^{1/3}Re = \frac{9.19}{Fo} = 9.19 \times 6326 = 58\ 136$$

4. Choose the impeller type and power number and calculate the Reynolds number. Use a pitched blade turbine with a power number of 1.80.

$$Re = \frac{58\ 136}{Po^{1/3}} = \frac{58\ 136}{1.8^{1/3}} = 47\ 792$$

5. Choose the impeller diameter and calculate the impeller speed. An impeller diameter of 50% the vessel diameter will be most energy efficient, so choose $D = 0.915$ m.

$$N = \frac{Re \cdot \mu}{\rho D^2} = \frac{47\ 792 \times 0.018}{1020 \times 0.915^2} = 1.01 \text{ rps}$$

6. The calculated speed is 1 rps, or 60 rpm, but this is not a standard gearbox output speed. The closest standard speeds are 56 and 68 rpm (see Table 6-2). With the same diameter, running at 56 rpm will increase the blend time by 7% while running at 68 rpm will decrease the blend time by 12%. Alternatively, the speed and diameter can be changed to give the desired blend time. This will be a judgment that the engineer has to make.
7. Design the agitator to run at 56 rpm accepting the slightly longer blend time; calculate the power input by the impeller and choose the motor size:

$$P = Po \cdot \rho N^3 D^5 = 1.8 \times 1020 \text{ kg/m}^3 \times \left(\frac{56}{60 \text{ s}}\right)^3 \times (0.915 \text{ m})^5 = 957 \text{ W}$$

The power input by the impeller is 957 W, or 1.28 hp. The next highest standard motor power would be 1.5 hp (see Table 6-2). This is acceptable since the power drawn by the impeller is roughly 85% of the available motor power.

8. The design is complete. The agitator will require a 1.5 hp motor with an output speed of 56 rpm. The impeller will be a pitched blade turbine 36 in. in diameter.

Example 9-2: Rating an Existing Agitator. An existing vessel and agitator are being considered for a new process. The vessel is 3 m in diameter and the liquid

depth will be 2.5 m. The fluid will have a viscosity of 500 mPa · s and a density of 980 kg/m^3. The impeller is a hydrofoil, with a power number of 0.33, 1.0 m in diameter and operating at 125 rpm. What will the blend time be?

SOLUTION

1. Determine the operating regime by calculating $Po^{1/3}Re$:

$$Po^{1/3}Re = Po^{1/3}\frac{\rho ND^2}{\mu} = 0.33^{1/3} \times \frac{980\ \text{kg/m}^3 \times (125/60\ \text{s}) \times (1.0\ \text{m})^2}{0.5\ \text{Pa} \cdot \text{s}}$$
$$= 2822$$

   The process will operate in the transitional regime since $Po^{1/3}Re < 6370$.

2. Calculate 1/Fo using the transitional correlation:

$$Po^{1/3}Re = \frac{183}{\sqrt{Fo}}$$
$$\frac{1}{\sqrt{Fo}} = \frac{Po^{1/3}Re}{183} = \frac{2822}{183} = 15.42$$
$$\frac{1}{Fo} = 237.8$$

3. Calculate the blend time:

$$\frac{1}{Fo} = \frac{\rho T^{1.5}H^{0.5}}{\mu\theta}$$
$$\theta = \frac{\rho T^{1.5}H^{0.5}}{\mu(1/Fo)} = \frac{980\ \text{kg/m}^3 \times (3.0\ \text{m})^{1.5} \times (2.5\ \text{m})^{0.5}}{0.5\ \text{Pa} \cdot \text{s} \times 237.8} = 67.7\ \text{s}$$

4. The blend time for 95% homogeneity will be 68 s. If a higher, or lower, degree of homogeneity is required, the appropriate correction factor can be calculated.

9-3 BLENDING OF NON-NEWTONIAN, SHEAR-THINNING FLUIDS IN THE TURBULENT AND TRANSITIONAL REGIMES

9-3.1 Shear-Thinning Fluids

Methods for designing agitators to blend Newtonian fluids were discussed in Section 9-2. Unfortunately, the vast majority of viscous fluids in the "real world" are non-Newtonian, and the Newtonian design rules must be modified to take account this fact. The most common type of non-Newtonian fluid exhibits shear-thinning behavior.

The behavior of a shear-thinning fluid can be described mathematically by the *power law*, which relates the shear stress in the fluid to the shear rate being exerted on it:

$$\tau = K\dot{\gamma}^n \tag{9-21}$$

so that from the definition of dynamic viscosity,

$$\mu_A = \frac{\tau}{\dot{\gamma}} = K\dot{\gamma}^{n-1} \tag{9-22}$$

where μ_A is the apparent viscosity of the fluid, and K and n are the consistency and flow behavior indices, respectively ($n < 1$ for a shear-thinning fluid). For this case quantitative relationships are available and these are discussed in this section.

The shear rate in an agitated vessel will vary with position, being highest near the impeller where the velocity gradients are steepest and low near the walls and surface. For a shear-thinning fluid this variation means that the apparent viscosity near the impeller is low, and near the wall, it is high. To estimate the blend time for a non-Newtonian fluid, the appropriate shear rate must be identified. This will then be used to estimate a value for the apparent viscosity of the fluid. Once this has been done, the Newtonian correlations can be used to estimate the blend time.

9-3.2 Literature Survey

Metzner and Otto (1957) developed the best-known definition of shear rate in an agitated vessel. They measured the power number for a variety of impellers in the laminar regime in Newtonian fluids and then repeated the measurements with shear-thinning fluids. They assumed that the power number was unaffected by the fluid's non-Newtonian behavior and that the Newtonian viscosity and shear-thinning apparent viscosity were equal for equal power number and Reynolds number. Once an estimate of the apparent viscosity is made, eq. (9-22) can be rearranged and the shear rate can be calculated from the power law model:

$$\dot{\gamma} = \left(\frac{\mu_A}{K}\right)^{1/(n-1)} = k_s N \tag{9-23}$$

Metzner and Otto concluded that the shear rate is proportional to the impeller speed with the constant of proportionality, k_S, taking a value between 10 and 15 for turbine impellers and 25 to 30 for close-clearance impellers. With this approach, the impeller Reynolds number can be modified to give

$$Re = \frac{\rho N D^2}{\mu_A} = \frac{\rho N^{(2-n)} D^2}{K k_S^{(n-1)}} \tag{9-24}$$

Strictly, this method is valid only in the laminar regime, where power number is inversely proportional to Reynolds number. Nagata et al. (1971) repeated these

experiments over an extended range of Reynolds numbers for a helical ribbon, anchor, flat blade, and Rushton turbine. They concluded that the Metzner and Otto shear rate did work in the laminar regime but failed in the transitional regime for the two turbine impellers (flat blade and Rushton). It did work for the two close-clearance impellers.

The Metzner and Otto method gives an estimate of the shear rate at the impeller based on the power measurement and the apparent viscosity at the impeller. Other processes in shear-thinning fluids, especially heat transfer, have also been studied where the shear rate at the impeller is not important. In this case the apparent viscosity and shear rate at the heat transfer surface are controlling and the Metzner–Otto method no longer applies.

Pollard and Kantyka (1969), Bourne et al. (1981), and Wang and Yu (1989) all concluded that in the laminar regime, the shear rate is proportional to the impeller speed, but in the transitional regime, the dependence on speed is more complicated. Generally, they found that the shear rate in the transitional regime is proportional to the square root of the power input per unit mass, indicating that turbulence is contributing to the generation of shear.

Wichterle et al. (1984) used an electrochemical technique to measure the shear rates on the surface of a Rushton turbine's blades for Newtonian and non-Newtonian fluids with a Reynolds number that varied between 1 and 10 000. They correlated their data by

$$\dot{\gamma}_m = (1 + 5.3n)^{1/n} Re_m^{1/(n+1)} N \tag{9-25}$$

where

$$Re_m = \frac{\rho N^{2-n} D^2}{K} \tag{9-26}$$

At low Reynolds numbers, the shear rate is proportional to impeller speed as reported by Metzner and Otto (1957). As Reynolds number increases, the exponent on the impeller speed increases from 1.0 to 1.5 (in a Newtonian fluid). This is due to the presence of shear stresses resulting from the turbulent fluctuating velocities that will start to appear. Note that eq. (9-26) does not contain the Metzner–Otto constant, k_S, because only one impeller type was used in the study.

9-3.3 Modifying the Newtonian Relationships for Shear-Thinning Fluids

The correlation for design of agitators for blending shear-thinning fluids in the turbulent and transitional regimes was developed at the fluid mixing processes consortium at Cranfield in the U.K. and is discussed in detail in Grenville (1992). The equipment and experimental technique described in Section 9-2.2 were used.

The Newtonian experiments had shown that in turbulent regime, the local blend times were the same throughout the vessel. As the viscosity increased and the Reynolds number decreased, the blend time measured behind the baffle increased significantly while those measured beneath the impeller and in the

middle of the vessel increased slightly compared with the turbulent values. The local blend time measured behind the baffle was controlling the blend time for the entire vessel. The approach that Grenville (1992) took to analyze the shear-thinning data was to determine the apparent viscosity of the fluid at the wall and use this value to calculate the values of Reynolds and Fourier numbers.

Bird et al. (1960) give an equation for the shear rate (tangential velocity gradient) on the wall of a baffled vessel and the pressure exerted on the baffles as a function of the torque on the agitator shaft:

$$\Lambda = \mu \iint_S R \left(\frac{\partial v_\theta}{\partial r} \right)_W dS + \iint_A R p_{baff} \, dA \tag{9-27}$$

Assuming that the shear rate is constant on the surfaces of the vessel wall and base, eq. (9-27) can be rewritten in terms of the shear stress at the vessel wall:

$$\Lambda = \tau_W \iint_S R \, dS + \iint_A R p_{baff} \, dA \tag{9-28}$$

The pressure exerted by the fluid on the baffles was estimated as

$$p_{baff} = \frac{\rho(\Delta v)^2}{2} \tag{9-29}$$

where Δv is the change in tangential velocity as the fluid impinges on the baffle.

Applying the appropriate integration limits, the shear stress at the wall in a vessel where $H = T$ with standard baffles and a torispherical bottom can be estimated from

$$\tau_W = \frac{1}{1.622} \left[\frac{\Lambda}{T^3} - 0.0638 \rho (\Delta v)^2 \right] \tag{9-30}$$

In order to use eq. (9-30), an estimate of the fluid velocity impinging on the baffle should be made, but the contribution of the pressure is small compared to the torque and, for engineering calculations, can be ignored. Thus, the estimated shear stress at the wall is

$$\tau_W = \frac{1}{1.622} \left(\frac{\Lambda}{T^3} \right) \tag{9-31}$$

The power law can then be used to determine the shear rate at the vessel wall and the apparent viscosity:

$$\tau_W = K \dot{\gamma}_W^n \tag{9-32}$$

$$\dot{\gamma}_W = \left(\frac{\tau_W}{K} \right)^{1/n} \tag{9-33}$$

$$\mu_W = K \dot{\gamma}_W^{n-1} \tag{9-34}$$

Once an estimate of the viscosity at the wall of the vessel has been made, Reynolds and Fourier numbers can be calculated and the method used for Newtonian fluids can be followed. It is important to remember that if any change

is made to the agitator's operation, the apparent viscosity at the wall must be recalculated.

9-3.4 Use of the Design Correlation

Again, there are two ways in which an engineer may have to use the blend time correlation; the first is to design a new agitator and the second is to rate an existing agitator for a new process. In both cases the extra step of estimating the fluid's apparent viscosity will be necessary.

The procedure for rating an existing agitator/vessel is relatively straightforward since the impeller type, speed, and diameter are known with the fluid physical properties. The torque on the agitator shaft can be calculated followed by the fluid's apparent viscosity at the wall. Then $Po^{1/3}Re_W$ can be calculated and the operating regime identified, and then $1/Fo_W$ can be calculated using the appropriate correlation. Finally, the blend time can be calculated.

The procedure for designing a new process is more complicated because the fluid's apparent viscosity at the wall is determined by the impeller type, diameter, and operating speed, which determine the shear stress and shear rate at the wall. The vessel size, fluid density, and desired blend time can be specified, but the viscosity is required in order to calculate $1/Fo_W$.

Since the apparent viscosity is a function of the impeller properties and $1/Fo_W$ cannot be calculated immediately, an iterative procedure must be made. This can be simplified because there are a limited number of possible gearbox output speeds. Once the impeller type and diameter have been chosen, the torque at each speed can be calculated followed by the shear stress and shear rate at the wall. Then the viscosity and $1/Fo_W$ can be calculated and the regime in which the impeller would operate can be identified. The appropriate correlation can then be used to calculate $Po^{1/3}Re_W$, and this can be rearranged to solve for the impeller speed. The condition where the output speed from rearranging $Po^{1/3}Re_W$ is just less than the input speed used to calculate $1/Fo_W$ is the one on which the design will be based. An example of this method is given in Section 9-3.7.

9-3.5 Impeller Efficiency

Again, the question of which impeller is the most efficient for blending can be answered by rearranging the blend time correlations. In the turbulent regime there is no dependence of blend time on viscosity, so the conclusions drawn for Newtonian fluids apply to non-Newtonian, shear-thinning fluids.

In the transitional regime the blend time is proportional to the fluid's apparent viscosity:

$$N\theta_{95} = \frac{183^2}{Po^{2/3}Re_W}\left(\frac{T}{D}\right)^2 \tag{9-35}$$

$$\theta_{95} \propto \left(\frac{T^3}{PoN^3D^5}\right)^{2/3}\frac{\mu_W}{\rho}D^{-2/3} \tag{9-36}$$

or

$$\theta_{95} \propto \left(\frac{T^3}{PoN^3D^5}\right)^{2/3} \frac{\mu_W}{\rho} \left(\frac{T}{D}\right)^{2/3} T^{-2/3} \tag{9-37}$$

$$\theta_{95} \propto \left(\frac{1}{\bar{\varepsilon}}\right)^{2/3} \frac{\mu_W}{\rho} \left(\frac{T}{D}\right)^{2/3} T^{-2/3} \tag{9-38}$$

Now the blend time is proportional to the viscosity of the fluid at the wall of the vessel. This in turn is dependent on the torque on the agitator's shaft; the higher the torque, the higher the shear stress and shear rate and the lower the fluid's apparent viscosity. So if two impellers of the same diameter are compared at the same power input per unit volume, the one with the lower power number, running at the higher speed, will give the longer blend time.

9-3.6 Cavern Formation and Size in Yield Stress Fluids

In very viscous, highly shear-thinning fluids (with n values on the order of 0.3 or less) whatever the physical reason for these particular rheological properties (e.g., mycelial fermentation broths, yogurt, high concentration, fine solid suspensions, emulsions, polymer solutions), agitation tends to cause cavern formation. A streak photograph of a cavern is shown in Figure 18-13. Thus, regions of liquid mixing and motion around the impeller are found, outside which the fluid is stagnant in dead zones or nearly so (Jaworski et al., 1994). In addition, there is no exchange of material (other than by diffusion) between the cavern and the bulk (Solomon et al., 1981). For Rushton turbines the cavern is usually cylindrical, centered on the agitator (Nienow and Elson, 1988) and of height/diameter ratio of 0.4. The shape is similar with the pitched blade turbine (Elson, 1988), the Scaba 6SRGT (Galindo and Nienow, 1993), and the Lightnin A315 (Galindo and Nienow, 1992), although with the latter the aspect ratio is a little higher (~ 0.6).

The boundary of the cavern can be defined as the surface where the local shear stress equals the fluid yield stress. If it is assumed that the predominant flow in the cavern is tangential [and LDA studies suggest that this is a reasonable approximation (Hirata et al., 1994)] and that the cavern shape, fluid yield stress, and impeller power number are known, the cavern size may be determined. A right circular cylinder of height H_c and diameter D_c centered on the impeller is a good model for the cavern shape, which allows for the effect of different impellers (Elson et al., 1986). Thus,

$$\left(\frac{D_C}{D}\right)^3 = \frac{Po \cdot \rho N^2 D^2}{\tau_y} \frac{1}{(H_c/D_c + \frac{1}{3})\pi^2} \tag{9-39}$$

Since the ratio of cavern height to diameter is typically 0.4, eq. (9-39) can be simplified to give

$$\left(\frac{D_C}{D}\right)^3 = \frac{1.36}{\pi^2} \frac{Po \cdot \rho N^2 D^2}{\tau_y} \tag{9-40}$$

This yield stress cavern model has been used by industrialists with some success (Etchells et al., 1987; Carpenter et al., 1993).

To use eq. (9-40) for agitator design, the cavern diameter must be set equal to the vessel diameter (i.e., the edge of the cavern must reach the vessel wall):

$$\left(\frac{T}{D}\right)^3 = \frac{1.36}{\pi^2}\frac{Po \cdot \rho N_C^2 D^2}{\tau_y} \tag{9-41}$$

Equation (9-41) can be rearranged to give

$$\frac{Po \cdot \rho N_C^2 D^5}{T^3} = \tau_y \frac{\pi^2}{1.36} \tag{9-42}$$

where N_C is the impeller speed when the cavern reached the vessel wall.

The term on the left-hand side of eq. (9-42) is the agitator shaft torque per unit volume. It does not matter what impeller type, diameter, and speed are chosen for the design, the torque must reach a lower limiting value in order for the cavern to reach the vessel wall. An agitator with a low power requirement can be designed by choosing a large diameter impeller ($\sim T/2$) with a higher power number. This will run at a lower speed, and since power is the product of torque and speed, a lower speed will result in less power required.

Once the cavern reaches the wall, it continues to rise up the vessel with increasing speed, but only rather slowly. Thus, very significant increases in energy dissipation rate are required to achieve motion everywhere. The most efficient way to ensure such motion is to use two impellers with D/T values of about 0.5 to 0.6 in a vessel of H/T and with one impeller being placed at $C = 0.25H$ and one at 0.75H. In this way, the two caverns approximately fill the vessel when either one produces a cavern that reaches the wall. The power requirement is just twice that required for a single impeller to reach the wall.

Recently, because of the difficulty of accurately determining the yield stress, a new model has been developed (Amanullah et al., 1998) based on assuming that a power law model with a low n value fits the flow curve. It also defines the cavern size by a minimum speed at its edge as the motion/no-motion boundary. As yet, an independent report has not been published confirming the effectiveness of this new approach. Finally, it should be noted that although there has been significant work dedicated to defining the size of the zones of motion in yield stress fluids, work has not been done to determine the blend time of the fluid inside the cavern.

9-3.7 Examples

Example 9-3: Designing a New Agitator. A new process is to be carried out in a baffled vessel that is 2 m in diameter operating with a liquid depth of 2 m. The fluid has a density of 995 kg/m^3 and a shear-thinning rheology. The consistency index, K, has a value of 5.25 Pa $\cdot$ s^n and a flow behavior index, n, of 0.654.

SOLUTION

1. Choose the impeller type and diameter. A large diameter impeller with a high power number will be best suited for blending a shear-thinning fluid. Choose a pitched blade turbine with Po = 1.75 and D = 1.0 m (or T/2).
2. Calculate the torque at a range of operating speeds. The torque is calculated from:

$$\Lambda = \frac{\mathrm{Po} \cdot \rho \mathrm{N}^2 \mathrm{D}^5}{2\pi} = \frac{1.75 \times 995\ \mathrm{kg/m^3} \times \mathrm{N}^2 \times (1.0\ \mathrm{m})^5}{2\pi} = 277.1\mathrm{N}^2\ \mathrm{N} \cdot \mathrm{m}$$

So for standard operating speeds between 30 and 155 rpm the torque will be as shown in Table 9-1.

Table 9-1

N (rpm)	Λ (N · m)	τ_W (Pa)	γ_W (s^{-1})
30	69	5.34	1.03
37	105	8.12	1.95
45	156	12.01	3.55
56	241	18.60	6.92
68	356	27.43	12.53
84	543	41.86	23.91
100	770	59.33	40.76
125	1203	92.70	80.64
155	1849	142.53	155.69

3. Calculate the shear stress and shear rate at the wall for each condition using

$$\tau_W = \frac{1}{1.622}\frac{\Lambda}{\mathrm{T}^3}$$

$$\dot{\gamma}_W = \left(\frac{\tau_W}{\mathrm{K}}\right)^{(1/n)}$$

Again, the results are given in Table 9.1.

4. Calculate the viscosity of the fluid at the wall and $1/\mathrm{Fo}_W$ using

$$\mu_W = \mathrm{K}\dot{\gamma}_W^{(n-1)}$$

$$\frac{1}{\mathrm{Fo}_W} = \frac{\rho \mathrm{T}^2}{\mu_W \theta}$$

as given in Table 9-2.

Table 9-2

N (rpm)	Λ (N · m)	τ_W (Pa)	γ_W (s^{-1})	μ_W (Pa · s)	$1/Fo_W$
30	69	5.34	1.03	5.20	15.30
37	105	8.12	1.95	4.17	19.10
45	156	12.01	3.55	3.39	23.49
56	241	18.60	6.92	2.69	29.61
68	356	27.43	12.53	2.19	36.36
84	543	41.86	23.91	1.75	45.47
100	770	59.33	40.76	1.46	54.69
125	1203	92.70	80.64	1.15	69.25
155	1849	142.53	155.69	0.92	86.95

5. Identify the regime in which the impeller would operate and calculate $Po^{1/3}Re_W$. In each case, $1/Fo_W$ is less than 1225, so the impeller operates in the transitional regime. Calculate $Po^{1/3}Re_W$ using

$$Po^{1/3}Re_W = \frac{183}{\sqrt{Fo_W}}$$

and Table 9-3.

Table 9-3

N (rpm)	μ_W (Pa · s)	$1/Fo_W$	$Po^{1/3}Re_W$
30	5.20	15.30	715.75
37	4.17	19.10	799.74
45	3.39	23.49	887.00
56	2.69	29.61	995.80
68	2.19	36.36	1103.52
84	1.75	45.47	1234.05
100	1.46	54.69	1353.30
125	1.15	69.25	1522.88
155	0.92	86.95	1706.44

6. For each case, calculate the impeller speed from

$$N = \frac{(Po^{1/3}Re_W)\mu_W}{Po^{1/3}\rho D^2}$$

as given in Table 9-4. The gearbox output speed at which the solution converges is 100 rpm, so this must be used to size the power required to run the agitator.

Table 9-4

N (rpm)	μ_W (Pa · s)	$1/Fo_W$	$Po^{1/3}Re_W$	N (rpm)
30	5.20	15.30	715.75	186
37	4.17	19.10	799.74	167
45	3.39	23.49	887.00	150
56	2.69	29.61	995.80	134
68	2.19	36.36	1103.52	121
84	1.75	45.47	1234.05	108
100	1.46	54.69	1353.30	98
125	1.15	69.25	1522.88	87
155	0.92	86.95	1706.44	78

7. Calculate the power drawn by the impeller and choose the appropriate motor size:

$$P = Po \cdot \rho N^3 D^5 = 1.75 \times 995 \text{ kg/m}^3 \times \left(\frac{100}{60 \text{ s}}\right)^3 \times (1.0 \text{ m})^5$$
$$= 8061 \text{ W (or } 10.80 \text{ hp)}$$

   The next standard motor size is 15 hp (see Table 6-2).
8. The design is complete. The agitator will require a 15 hp motor with an output speed of 100 rpm. The impeller will be a pitched blade turbine 1.0 m in diameter.

Example 9-4: Rating an Existing Agitator. An existing vessel and agitator are being considered for a new process. The vessel is 3 m in diameter and the liquid depth will be 3 m. The fluid is shear-thinning with a power law constant of $K = 8.98 \text{ Pa} \cdot \text{s}^n$, a power law index of $n = 0.467$, and a density of 1050 kg/m^3. The impeller is a hydrofoil, with a power number of 0.33, 1.5 m in diameter, and operating at 125 rpm. What will the blend time be?

SOLUTION

1. Calculate the torque on the agitator shaft:

$$\Lambda = \frac{Po \cdot \rho N^2 D^5}{2\pi} = \frac{0.33 \times 1050 \text{ kg/m}^3 \times (125/60 \text{ s})^2 \times (1.5 \text{ m})^5}{2\pi}$$
$$= 1817.6 \text{ N} \cdot \text{m}$$

2. Calculate the shear stress at the wall:

$$\tau_W = \frac{1}{1.622}\left(\frac{\Lambda}{T^3}\right) = \frac{1}{1.622} \times \frac{1817.6 \text{ N} \cdot \text{m}}{(3 \text{ m})^3} = 41.50 \text{ Pa}$$

3. Determine the shear rate at the wall:

$$\dot{\gamma}_W = \left(\frac{\tau_W}{K}\right)^{1/n} = \left(\frac{41.50}{8.98}\right)^{1/0.467} = 26.51 \text{ s}^{-1}$$

4. Determine the apparent viscosity at the wall:

$$\mu_W = K\dot{\gamma}_W^{n-1} = 8.98 \times 26.51^{0.467-1} = 1.565 \text{ Pa} \cdot \text{s}$$

5. Determine the operating regime by calculating $Po^{1/3}Re_W$:

$$Po^{1/3}Re_W = Po^{1/3}\frac{\rho ND^2}{\mu_W}$$

$$= 0.33^{1/3} \times \frac{1050 \text{ kg/m}^3 \times (125/60 \text{ s}) \times (1.5 \text{ m})^2}{1.565 \text{ Pa} \cdot \text{s}} = 2173$$

The process will operate in the transitional regime since $Po^{1/3}Re_W < 6370$.

6. Calculate $1/Fo_W$ using the transitional correlation

$$Po^{1/3}Re_W = \frac{183}{\sqrt{Fo_W}}$$

$$\frac{1}{\sqrt{Fo_W}} = \frac{Po^{1/3}Re_W}{183} = \frac{2176}{183} = 11.89$$

$$\frac{1}{Fo_W} = 141.4$$

7. Calculate the blend time:

$$\frac{1}{Fo_W} = \frac{\rho T^2}{\mu_W \theta}$$

$$\theta = \frac{\rho T^2}{\mu_W(1/Fo)} = \frac{1050 \text{ kg/m}^3 \times (3.0 \text{ m})^2}{1.565 \text{ Pa} \cdot \text{s} \times 141.1} = 42.8 \text{ s}$$

The blend time for 95% homogeneity will be 43 s.

Example 9-5: Minimum Speed for Agitation of a Yield Stress Fluid. A fluid with a density of 1560 kg/m^3 and exhibiting a yield stress of 18 Pa is to be stored in a vessel 3 m in diameter with a maximum operating depth of 2.3 m. Design an agitator that will eliminate stagnant zones in the vessel.

SOLUTION

1. Choose the impeller type and diameter. A large diameter impeller ($\sim$T/2) with a higher power number will operate at a lower speed and power. Choose a pitched blade turbine (Po = 1.8), 1.5 m in diameter.

2. Calculate the minimum speed, N_C, for the cavern to reach the vessel wall from

$$\left(\frac{T}{D}\right)^3 = \frac{1.36}{\pi^2}\left(\frac{Po \cdot \rho N_C^2 D^2}{\tau_y}\right)$$

$$N_C = \left(\tau_y \frac{\pi^2}{1.36}\frac{T^3}{Po \cdot \rho D^5}\right)^{1/2}$$

$$= \left(18\ Pa \times \frac{\pi^2}{1.36} \times \frac{(3.0\ m)^3}{1.8 \times 1560\ kg/m^3 \times (1.5\ m)^5}\right)^{1/2} = 0.407\ rps$$

The minimum speed will be 24.4 rpm; from Table 6-2 30 rpm is the next highest standard speed.

3. Determine the number and location of the impeller(s). The height of the cavern will be approximately 40% of its diameter, in this case 1.2 m. Two impellers located at a clearance off the vessel base of 0.6 and 1.8 m will produce two intersecting caverns to a total height of 2.4 m which is higher than the maximum operating level.
4. Calculate the power drawn by the two impellers and choose the motor size. The power drawn will be calculated from

$$P = 2Po \cdot \rho N^3 D^5 = 2 \times 1.8 \times 1560\ kg/m^3 \times \left(\frac{30}{60\ s}\right)^3 \times (1.5\ m)^5$$

$$= 5331\ W\ (or\ 7.14\ hp)$$

The next standard motor size is 7.5 hp, but this would mean that the impeller power draw will be 95% of the motor power. Choose a 10 hp motor.

5. The design is complete. The agitator will require a 10 hp motor with an output speed of 30 rpm. The impellers will be two pitched blade turbines 1.5 m in diameter located 0.6 and 1.8 m above the vessel base.

9-4 BLENDING IN THE LAMINAR REGIME

Turbine and hydrofoil impellers operating in the turbulent and transitional regimes rely on entrainment to move fluid from the impeller region to the vessel walls and surface. As the viscosity of the fluid increases, primary flow generated by the impeller and level of entrainment are reduced until the regions away from the impeller become "stagnant."

In the transitional regime the dimensionless blend time, $N\theta$, is inversely proportional to Reynolds number. As the fluid's viscosity increases (and Reynolds number decreases) a value is reached where the dimensionless blend time becomes more sensitive to changes in viscosity. At this value of Reynolds number, the decision of whether to use a turbine impeller or to change to an

impeller better suited to operation in the laminar regime must be made. The differences between these impellers are illustrated on the Visual Mixing CD. At very low Reynolds numbers, one of these impellers will be used. In this section we cover the calculations that can be made to determine if the process operates in the laminar regime, and if it does, what impeller to use and how to design it.

9-4.1 Identifying the Operating Regime for Viscous Blending

Two methods have been used to identify the boundary between transitional and laminar blending, and they give similar results for the value of Reynolds number at the boundary. Wichterle and Wein (1981) made visualization studies of the flow in vessels agitated by Rushton and pitched blade turbines. They defined two Reynolds numbers: the value when motion first appears and the value when all stagnant zones disappear. The second definition is used here:

$$\mathrm{Re_{TL}} = \left(\frac{1.8\ \mathrm{T}}{\mathrm{aD}}\right)^2 \tag{9-43}$$

The value of a can be calculated from

$$\mathrm{a} = 0.375\mathrm{Po}^{1/3} \tag{9-44}$$

So, for example, a pitched blade turbine with a power number of 1.8 and diameter equal to T/2 will have a value of $\mathrm{Re_{TL}}$ of 62.

Hoogendoorn and den Hartog (1967) measured blend times for a variety of impellers. They found that when the dimensionless blend time data were plotted, the exponent on Reynolds number changed from -1 to -10 at a value of Reynolds number of 170 for a Rushton turbine (i.e., the blend time became highly sensitive to the value of viscosity for $\mathrm{Re} < 170$). Johnson (1967) found that the exponent was -13.

Hoogendoorn and den Hartog proposed that the boundary between the laminar and transitional regimes could be estimated for all impellers by

$$\frac{1}{\mathrm{Fo}} = 1 \text{ at } \mathrm{Re_{TL}} \tag{9-45}$$

This agrees well with the conclusions of Zlokarnik (1967), who concluded that the boundary occurs at a value of 0.25. Substituting the value of 1/Fo from eq. (9-45) into (9-6) and rearranging gives

$$\mathrm{Re_{TL}} = \frac{183}{\mathrm{Po}^{1/3}}\frac{1}{\sqrt{\mathrm{Fo}}} = \frac{183}{\mathrm{Po}^{1/3}} \tag{9-46}$$

For the pitched blade turbine with a power number of 1.8, eq. (9-46) predicts that $\mathrm{Re_{TL}}$ will be 150 (Hoogendoorn and den Hartog, 1967) or 75 (Zlokarnik, 1967). Use of an impeller specifically designed for laminar operation must be

considered when the Reynolds number is in the range 100 to 200. At lower Reynolds numbers ($< \sim 50$) it becomes easier to make the decision.

9-4.2 Impeller Selection

The most commonly used impeller for laminar blending applications is the helical ribbon. Other impeller types have been studied, including anchors and helical screws, but the helical ribbon is most effective. A helical ribbon impeller will have a large diameter, typically 90 to 95% of the vessel diameter. This ensures that the fluid is "positively displaced" by the ribbons. This is important because there is no mixing due to entrainment by eddies in the laminar regime.

A typical helical ribbon is shown in Figure 6-31. Although different numbers of ribbons can be supplied, it is usual for the impeller to have two. This ensures that the hydraulic forces exerted on the shaft are balanced. The pitch (the ribbon height of one 360° turn) is usually equal to the impeller diameter, and the width of a ribbon blade is typically 10% of the impeller diameter. A tighter pitch and wider ribbon will increase the power draw.

9-4.3 Estimation of Power Draw

The power drawn by an impeller operating in the laminar regime is calculated from

$$Po = \frac{K_P}{Re} \tag{9-47}$$

The power drawn by an impeller in the laminar regime can be calculated from

$$P = Po \cdot \rho N^3 D^5 = \frac{K_P \mu}{\rho N D^2} \rho N^3 D^5 = K_P \mu N^2 D^3 \tag{9-48}$$

The power drawn by an impeller is proportional to the fluid viscosity.

The constant K_P is a function of the impeller's geometry and a variety of correlations have been produced to relate its value to the geometrical ratios of a helical ribbon impeller. There are a number of correlations available in the literature for estimating the value of K_P. For example, Shamlou and Edwards (1985) correlated their data by

$$K_P = 150 \frac{h}{D} \left(\frac{p}{D}\right)^{-0.50} \left(\frac{c}{w}\right)^{0.33} n_b^{0.50} \tag{9-49}$$

Brito-de la Fuente et al. (1997) did not vary D/T and as a consequence, c/D, and found that

$$K_P = 173.1 \left(\frac{p}{D}\right)^{-0.72} \left(\frac{w}{D}\right)^{0.14} \tag{9-50}$$

Rieger et al. (1988) reported that

$$K_P = 82.8 \frac{h}{D} \left(\frac{c}{D}\right)^{-0.38} \left(\frac{p}{D}\right)^{-0.35} \left(\frac{w}{D}\right)^{0.20} n_b^{0.78} \tag{9-51}$$

Their correlation included data from eight geometries that they measured themselves and 69 others that were available in the literature. Given the similarities between the various correlations, using this version will give a good estimate for K_P and will account for all possible geometrical variations. It is also based on total of 77 experimental observations, which increases the level of confidence in its use.

9-4.4 Estimation of Blend Time

The dimensionless blend time, $N\theta$, is a constant for a helical ribbon operating in the laminar regime (see, e.g., Hoogendoorn and den Hartog, 1967; Johnson, 1967; Rieger et al., 1986). This means that the blend time is independent of Reynolds number and the fluid viscosity, so that even if the fluid is shear-thinning the blend time will not be affected by the rheological behavior. This is not true for visco-elastic behavior.

Grenville et al. (2001) took the data of Rieger et al. (1986) and found that the dimensionless blend time could be correlated with the constant K_P by

$$N\theta = 896 \times 10^3 K_P^{-1.69} \tag{9-52}$$

The standard error for the constant is $\pm 17\%$.

The higher the value of K_P, the lower the dimensionless blend time. Grenville et al. (2001) also found that an impeller with a high K_P value was the most energy efficient geometry (i.e., gave the shortest blend time for a given power input).

9-4.5 Effect of Shear-Thinning Behavior

The power drawn by any impeller in the laminar regime is proportional to the fluid viscosity, so an estimate of the apparent viscosity must be made for a shear-thinning fluid. Since the impeller is operating in the laminar regime, the Metzner and Otto approach to estimating the shear rate is valid, and for helical ribbons, the constant k_S has a value of 30. Shamlou and Edwards (1985) found that there is a weak effect of the gap between the ribbon and the vessel wall on this value, but for engineering calculations, the value of 30 is accurate enough.

9-4.6 Design Example

Example 9-6. A small volume of liquid is to be added to a large volume of viscous fluid in a vessel that is 2 m in diameter. The depth will also be 2 m. The fluid has a density of 990 kg/m^3 and is shear-thinning with a consistency index of 1450 Pa $\cdot$ s^n and a flow behavior index of 0.45. A sample will be taken after 10 min to check that the fluid is homogeneous. Design an agitator for this process.

SOLUTION

Start by assuming a standard helical ribbon impeller with two blades, $p/D = h/D = 1$; $D/T = 0.95$; $w/D = 0.1$. From eq. (9-51), $K_p = 357$. From eq. (9-52)

$$N = \frac{8.96 \times 10^5}{(357)^{1.69}(600\ \text{s})} = 0.07\ \text{s}^{-1} = 4\ \text{rpm}$$

The closest standard speed is 16.5 rpm (Table 6-2). This is much higher than the 4 rpm required and will result in a higher-than-necessary power consumption. Decrease the impeller diameter to $D/T = 0.9$, keeping everything else the same. The new $N = 7$ rpm is much closer to the smallest available speed of 16.5 rpm (0.275 rps).

The next step is to calculate the Reynolds number using the apparent viscosity and the Metzner–Otto equation. For helical ribbon impellers, $k_s = 30$:

$$\dot{\gamma} = 30N = 8.25\ \text{s}^{-1}$$

$$\mu_{app} = 1450\dot{\gamma}^{-0.55} = 454\ \text{Pa} \cdot \text{s}$$

$$\text{Re} = \frac{\rho N D^2}{\mu_{app}} = \frac{990\ \text{kg/m}^3 \times 0.275\ \text{s}^{-1} \times (1.8\ \text{m})^2}{454\ \text{Pa} \cdot \text{s}} = 1.94$$

This is far into the laminar regime; check the Re_{TL}. From eq. (9-46), $Re_{TL} = 35$, so the helical ribbon is a good choice. Because a helical ribbon impeller was selected, caverns are not a concern in this application. The power draw will be

$$P = Po \cdot \rho N^3 D^5 = 53.9\ \text{kW} = 72\ \text{hp}$$

The closest standard motor size is 75 hp, and the next largest is 100 hp (Table 6-2). A slight further reduction in the impeller diameter to 0.88T reduces the power draw to 62 hp, which is a better match for the motor size. The blend time is still well below the requirement of 10 min.

9-5 JET MIXING IN TANKS

Mixing of fluids requires the input of mechanical energy to achieve a process result, and previous sections in this chapter have dealt with equipment that consists of an impeller, or impellers, attached to a rotating shaft. An alternative method for getting energy into the fluid is to generate a high velocity jet of fluid in the vessel. Vertically oriented jets are illustrated on the Visual Mixing CD. The jet entrains and mixes the surrounding fluid and the mechanical energy is supplied from a pump. The rules for designing jet mixers for use in low viscosity turbulent applications are very well defined and can be used with a great deal of confidence.

Jet mixers are commonly used in large storage tanks, where the contents must be homogenized, but the required blend time can be on the order of hours rather

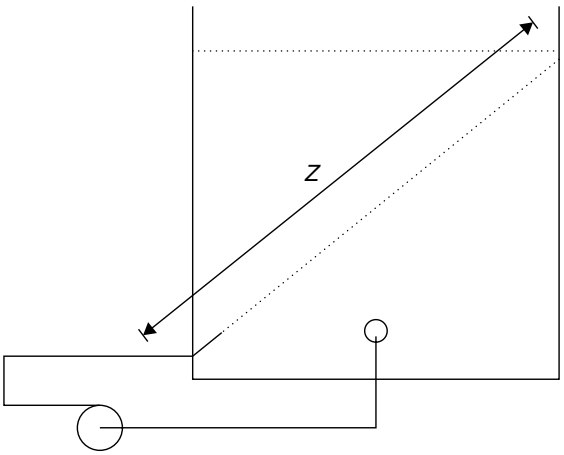

Figure 9-1 Jet mixer configuration for blending operations.

than minutes or seconds. This will be the main area covered in this chapter. When used in large storage tanks the jet usually enters from the side of the vessel close to the base and is directed toward the opposite top corner (see Figure 9-1).

Jet mixers are driven by pumps that can be located on the ground next to the vessel, giving easy access for maintenance. The vessel will often need a pump for filling and emptying, and this pump can also be used for the jet mixer, thus reducing the capital investment needed, especially if an agitator is being considered.

9-5.1 Literature Review

A number of studies have been done over the years measuring blend time in jet mixed vessels. During World War II, Fossett and Prosser (1949) examined the blending of tetraethyl lead (TEL) into aviation fuel in underground storage tanks. Their main concern was to ensure that the dense TEL stream was well mixed with the fuel, but they proposed a correlation for estimating the blend time as a function of the vessel diameter, nozzle diameter, and jet velocity:

$$\theta \propto \frac{T^2}{UD} \tag{9-53}$$

or in dimensionless terms,

$$\frac{U\theta}{D} \propto \left(\frac{T}{D}\right)^2 \tag{9-54}$$

This correlation predicts that in the turbulent regime, the dimensionless blend time is independent of the jet Reynolds number.

Fox and Gex (1956) also measured blend times in jet mixed tanks and proposed a correlation that included an effect of the jet Reynolds and Froude numbers:

$$\frac{U\theta}{D} \propto \left(\frac{Fr}{Re}\right)^{1/6} \frac{TH^{1/2}}{D^{3/2}} \tag{9-55}$$

Van de Vusse (1959) measured blend times in a 12 000 m^3 vessel and concluded that the Fossett and Prosser form of correlation best fit his data and that the Fox and Gex correlation underpredicted the measured blend times. Several other workers have measured blend times in jet-mixed vessels, with most finding that the Fossett and Prosser correlation fit their data. These include Okita and Oyama (1963) and Ràcz and Wassink (1973).

Grenville et al. (1992) measured blend times in three jet-mixed vessels 0.61, 1.68, and 3.98 m in diameter and force-fit the data into the two correlations that had been proposed in the literature. They found that the Fossett and Prosser correlation fit the data with a standard deviation of 8.15%, whereas for the Fox and Gex correlation the standard deviation was 18.9%. Also, a regression of the data showed that the Fossett and Prosser correlation was, in fact, the best fit for the data.

9-5.2 Jet Mixer Design Method

The correlations developed for estimating blend time in jet-mixed vessels were based on regression analysis of experimental data but without any physical understanding of the phenomena that control the process. Grenville and Tilton (1996) proposed that the overall blend time in a jet-mixed vessel would be determined from the mixing in the region of the vessel where the local mixing rate was slowest. The mixing rate at the end of the jet path could be estimated and compared with the mixing rate for the entire vessel.

The mixing rate can be estimated using the Corrsin (1964) time scale (see Chapter 2), where the turbulent energy dissipation rate is calculated at the end of the jet path and the appropriate length scale is the jet's free path, Z:

$$\theta = K_Z \left(\frac{\varepsilon_Z}{Z^2}\right)^x \tag{9-56}$$

where K_Z is a dimensionless constant. If the data fit the Corrsin model, the exponent, x, would be $-\frac{1}{3}$.

The turbulent kinetic energy dissipation rate at the end of the jet is estimated from the jet's centerline velocity and diameter at the end of its free path:

$$\varepsilon_Z = A_Z \frac{U_Z^3}{D_Z} \tag{9-57}$$

The velocity on the centerline of a turbulent jet can be estimated from Rajaratnam (1986):

$$U_Z = 6\frac{UD}{Z} \tag{9-58}$$

As the jet moves away from the nozzle it expands and slows down as it entrains the surrounding fluid. Its momentum is conserved. The relationship between the jet velocity at the nozzle, the nozzle diameter, and the jet's velocity and diameter at any distance along its path will be

$$UD = U_Z D_Z \tag{9-59}$$

Substituting eqs. (9-58) and (9-59) into (9-57), it can be shown that

$$\varepsilon_Z \propto \frac{(UD)^3}{Z^4} \tag{9-60}$$

and thus:

$$\theta \propto \left[\frac{(UD)^3}{Z^6}\right]^x \tag{9-61}$$

So the turbulent kinetic energy dissipation rate at the end of the jet can be calculated from quantities that are known: the jet velocity at the nozzle, the nozzle diameter, and the path length.

Blend time data measured in three scales of vessel were fitted to this relationship and the regression showed that the exponent was $-\frac{1}{3}$ as expected. Equation (9-61) is rearranged using $x = -\frac{1}{3}$ to give

$$\theta = K_Z \frac{Z^2}{UD} \tag{9-62}$$

for the conditions:

- $Re > 10\ 000$ (turbulent flow)
- $0.2 < H/T < 2.0$
- $0.178 < V < 1200\ m^3$
- $1.32 \times 10^{-2} < (UD/Z) < 0.137$ m/s
- $86 < Z/D < 753$

The constant K_Z has a value of 3.00 with a standard deviation of $\pm 11.0\%$.

Equation (9-62) can be rearranged into two dimensionless groups:

$$UD = K_Z \frac{Z^2}{\theta} \tag{9-63}$$

Multiplying both sides of eq. (9-63) by ρ/μ yields

$$\frac{\rho UD}{\mu} = K_Z \frac{\rho Z^2}{\mu\theta} \tag{9-64}$$

The dimensionless group on the left-hand side of eq. (9-64) is the jet Reynolds number and the group on the right-hand side is the reciprocal of Fourier number, as used for agitator design and rating calculations.

$$Re = \frac{K_Z}{Fo} \tag{9-65}$$

Expressing the correlation in this way makes it very useful for design since the properties of the jet are separated from the properties of the mixing duty (the blend time, vessel size, and liquid physical properties).

The correlation can be used in two ways; the first is simply to use the value $K_Z = 3.00$ with no account taken of the standard deviation of the experimental results. The second, taking account of the standard deviation, allows a level of confidence to be included in the design procedure. Approximately 67% of observations will lie within ± 1 standard deviation. Similarly, 95% lie within ± 2 standard deviations and 99% lie within ± 3 standard deviations. So if the second approach is to be taken, including a level of confidence, the constant K_Z in eq. (9-65) can be defined as $3.00 + 0.33$ s, where $s = 1$ for 67% confidence, $s = 2$ for 95% confidence, and $s = 3$ for 99% confidence. Examples of the correlation's use are given in Section 9-5.3.

9-5.3 Jet Mixer Design Steps

There are two ways in which the correlation for blend times can be used:

1. Designing a new vessel and jet mixer
2. Rating an existing vessel and jet mixer

9-5.3.1 Designing a New Jet Mixer. For a new application, the vessel dimensions and required blend time will be defined. The Fourier number can be calculated immediately, followed by the required jet Reynolds number. A jet velocity needs to be chosen at this point and a typical value would be 10 m/s. Once this is done, the nozzle diameter can be calculated from the jet Re, followed by the pressure drop and the pump flow rate. The jet nozzle should be constructed from standard pipe, and sizes are given in Perry and Green (1984). Choose the next larger standard pipe above the calculated diameter and recalculate the pressure drop and flow rate. This will give a shorter blend time, so it will be possible to use a lower jet velocity with this standard pipe size. If the tank operates in continuous mode, the flow through the vessel may be used to drive the jet mixer (see Example 9-8).

9-5.3.2 Pump Sizing. Using the design correlation to size a jet mixer will determine what the required flow rate through the nozzle has to be to achieve the desired blend time. In order to specify the pump, it is necessary to know the pressure drop through the system. It is quite likely that the actual operating point on the pump curve will not give exactly the flow rate specified, so the pump curve and the mixing curve must be combined to find the operating conditions for the system. The pump curve for a centrifugal pump can be fitted to a quadratic equation with the head on the y-axis and flow rate on the x-axis. The mixing time correlation can be expressed in terms of the flow rate and the head loss through the piping system and mixer nozzle.

9-5.4 Design Examples

Example 9-7: Design of a New Jet Mixer. A monomer storage vessel is 10 m in diameter with a straight-side height of 8 m. Thirty minutes after delivery of a fresh shipment of monomer, the vessel contents are sampled and analyzed. A jet mixer will be installed in the vessel to blend the new shipment with the existing fluid. The monomer has a density of 850 kg/m^3 and viscosity of 1.2 mPa · s. Design the jet mixer.

SOLUTION

1. Calculate the jet path length. For an optimum jet geometry with maximized jet path length,

$$Z = \sqrt{H^2 + T^2} = \sqrt{8^2 + 10^2} = 12.81 \text{ m}$$

2. The Fourier number can be calculated immediately since the required blend time has been defined as 30 min:

$$\text{Fo} = \frac{\mu\theta}{\rho Z^2} = \frac{1.2 \times 10^{-3} \text{ Pa} \cdot \text{s} \times (30 \times 60 \text{ s})}{850 \text{ kg/m}^3 \times (12.81 \text{ m})^2} = 1.55 \times 10^{-5}$$

3. Now calculate the required jet Reynolds number using K = 3.00.

$$\text{Re} = \frac{K_Z}{\text{Fo}} = \frac{3.00}{1.55 \times 10^{-5}} = 1.935 \times 10^5$$

4. Setting the jet velocity equal to 10 m/s, calculate the required nozzle diameter:

$$D = \frac{\text{Re} \cdot \mu}{\rho U} = \frac{(1.935 \times 10^5) \times 1.2 \times 10^{-3} \text{ Pa} \cdot \text{s}}{850 \text{ kg/m}^3 \times 10 \text{ m/s}} = 0.027 \text{ m}$$

   The next larger standard pipe size is 0.035 m (1.25 in. schedule 40 pipe). The jet path/nozzle diameter ratio Z/D = 366, which is acceptable.

5. Calculate the required flow rate:

$$Q = \frac{\pi}{4} U D^2 = \frac{\pi}{4} \times 10 \text{ m/s} \times (0.035 \text{ m})^2 = 9.62 \times 10^{-3} \text{ m}^3/\text{s}$$

   (or 152 US gal/min).

6. Finally, estimate the head loss through the piping and jet nozzle:

$$h_L = 2.5 \frac{U^2}{2g} = 2.5 \times \frac{(10 \text{ m/s})^2}{2 \times 9.81 \text{ m/s}^2} = 12.75 \text{ m of fluid}$$

   Once the piping has been laid out, a more rigorous pressure drop calculation can be made to size the pump.

If a 95% confidence level is to be applied to this design, the constant K_Z in step 3 would be 3.66 (i.e., $3 + 2 \times 0.33$).

Example 9-8: Design of a Jet Mixer for an Existing Process. An effluent stream is pumped to a large vessel prior to treatment in aerobic digesters. The flow rate can range between 4 and 7 m^3/min. The vessel is 36 m in diameter and has an operating volume of 8000 m^3, giving a residence time of about 1 day. To improve the operation of the digesters, it has been decided that the contents of the vessel must be blended to prevent spikes in effluent concentration from reaching the microorganisms. Can the pump provide enough flow to blend the vessel contents in a short enough time?

SOLUTION

1. Calculate the nozzle diameter. Choose a jet velocity of 10 m/s at the highest flow rate as a starting point for the calculation:

$$D = \sqrt{\frac{Q}{(\pi/4)U}} = \sqrt{\frac{7\ m^3/60\ s}{(\pi/4) \times 10\ m/s}} = 0.122\ m$$

2. Calculate the Reynolds number. The fluid is water with a density of 1000 kg/m^3 and a viscosity of 1.0 mPa · s:

$$Re = \frac{\rho UD}{\mu} = \frac{1000\ kg/m^3 \times 10\ m/s \times 0.122\ m}{0.001\ Pa \cdot s} = 1.22 \times 10^6$$

3. Calculate the Fourier number. The jet is turbulent, so $K_Z = 3.00$ and

$$Fo = \frac{3.00}{Re} = \frac{3.00}{1.22 \times 10^6} = 2.46 \times 10^{-6}$$

4. Calculate the jet path length. First, the liquid level must be calculated:

$$H = \frac{V}{(\pi/4)T^2} = \frac{8000\ m^3}{(\pi/4) \times (36\ m)^2} = 7.86\ m$$

The jet path length is

$$Z = \sqrt{H^2 + T^2} = \sqrt{(7.86\ m)^2 + (36\ m)^2} = 36.85\ m$$

5. Calculate the blend time:

$$\theta = \frac{Fo \cdot \rho Z^2}{\mu} = 3340\ s = 56\ min$$

This is much less than the residence time, so the jet mixer will be effective at the high flow rate. Repeating the calculations for the low flow rate gives

$$U = \frac{4}{60(\pi/4)(0.122)^2} = 5.7 \text{ m/s}$$

$$Re = 7 \times 10^5 \qquad \text{turbulent since } Re > 10\,000$$

$$Fo = 4.3 \times 10^{-6}$$

$$\theta = 5840 \text{ s} = 97 \text{ min}$$

This is still much less than 10% of the mean residence time, so the jet mixer will be sufficient.

NOMENCLATURE

A	area of baffle (m^2)
A_Z	dimensionless constant
c	helical ribbon impeller wall clearance (m)
c'	concentration fluctuation (concentration units)
C	impeller off-bottom clearance (m)
D	impeller diameter (m)
D	jet diameter at the nozzle (m)
D_c	cavern diameter (m)
D_z	jet diameter at the end of the jet path (m)
Fo	Fourier number, $\mu\theta/\rho T^2$
Fo_{TT}	transition to turbulent Fourier number
Fo_w	Fourier number at the wall
F_r	jet Froude number
h	helical ribbon impeller height (m)
h_L	head loss through the jet piping (m)
H	fluid height (m)
H_c	cavern height (m)
k	blending rate constant (s^{-1})
k_s	Metzner–Otto constant
K	power law constant or consistency index ($Pa \cdot s^n$)
K_p	$P_o \cdot R_e$ in the laminar regime
K_Z	constant for jet mixing time correlation (= 3.00)
n	power law exponent or flow behavior index
n_b	number of blades, helical ribbon impeller
N	impeller rotational speed (rps)
N_c	impeller speed at which the cavern reaches the wall (rps)
p	helical ribbon impeller pitch (m per 360° rotation)
p_{baff}	pressure on the baffles (Pa)
Po	power number, $P/\rho N^3 D^5$

Q volumetric flow rate through the nozzle (m^3/s)
r radius (m)
R tank radius (m)
Re impeller Reynolds number, ND^2/ν
Re_{TL} transition to laminar Reynolds number
Re_{TT} transition to turbulent Reynolds number
Re_w Reynolds number at the wall
S wall area (m^2)
t time (s)
T tank diameter (m)
U jet velocity at the nozzle (m/s)
U_z velocity at the end of the jet (m/s)
V vessel volume (m^3)
v tangential velocity (m/s)
w helical ribbon impeller blade width (m)
x relative magnitude of the concentration fluctuation
Z jet path length in a jet mixer (m)

Greek Symbols

$\dot{\gamma}_w$ wall shear rate (s^{-1})
$\dot{\gamma}$ shear rate (s^{-1})
$\bar{\varepsilon}$ power dissipated per unit mass, $Po \cdot N^3D^5/V$ (m^2/s^3)
ε_Z turbulent energy dissipation rate at the end of the jet (m^2/s^3)
θ_{95} blend time to 95% reduction in variance (s)
θ_M blend time to 95% reduction in variance for multiple impellers (s)
Λ torque on the shaft ($N \cdot m$)
μ dynamic viscosity ($Pa \cdot s$ or $kg/m \cdot s$)
μ_A apparent viscosity ($Pa \cdot s$)
μ_w viscosity at the wall ($Pa \cdot s$)
ρ fluid density (kg/m^3)
τ shear stress (N/m^2 or Pa)
τ_W shear stress at the wall (N/m^2 or Pa)
τ_Y yield stress (Pa)

REFERENCES

Amanullah, A., S. J. Hjorth, and A. W. Nienow (1998). A new mathematical model to predict cavern diameters in highly shear thinning, power law liquids using axial flow impellers, *Chem. Eng. Sci.*, **53**, 455–469.

Bird, R. B., W. E. Stewart, and E. N. Lightfoot (1960). *Transport Phenomena*, Wiley, New York, Chap. 6, p. 205.

Bourne, J. R., M. Buerli, and W. Regenass (1981). Power and heat transfer to agitated suspensions: use of heat flow calorimetry, *Chem. Eng. Sci.*, **36**, 782–784.

Brito-de la Fuente, E., L. Choplin, and P. A. Tanguy (1997). Mixing with helical ribbons: effect of highly shear-thinning behaviour and impeller selection, *Trans. Inst. Chem. Eng.*, **75**, 45–52.

Carpenter, K. J., P. C. Lines, R. Aldington, A. Keron, and W. A. J. Hindson (1993). Two examples of designing full scale reactors for multi-stage synthesis involving non-Newtonian mixtures, presented at the AIChE Annual Meeting, St. Louis, MO.

Cooke, M., J. C. Middleton, and J. R. Bush (1988). Mixing and mass transfer in filamentous fermentations, *Proc. 2nd International Conference on Bioreactor Fluid Dynamics*, pp. 37–64.

Corrsin, S. (1964). The isotropic turbulent mixer: II. Arbitrary Schmidt number, *AIChE J.*, **9**, 870–877.

Cronin, D. G., A. W. Nienow, and G. W. Moody (1994). An experimental study of the mixing in a proto-fermenter agitated by dual Rushton turbines, *Food Bioprod. Process. (Trans. Inst. Chem. Eng. C)*, **72**, 35–40.

Elson, T. P. (1988). Mixing of fluids possessing a yield stress, *Proc 6th European Conference on Mixing*, pp. 485–492.

Elson, T. P., D. J. Cheesman, and A. W. Nienow (1986). X-ray studies of cavern sizes and mixing performance with fluids possessing a yield stress, *Chem. Eng. Sci.*, **41**, 2555–2562.

Etchells, A. W., W. N. Ford, and D. G. R. Short (1987). *Fluid Mixing 3, Inst. Chem. Eng. Symp. Ser.*, **108**, pp. 1–10.

Fossett, H., and L. E. Prosser (1949). The application of free jets to mixing of fluids in bulk, *Proc. Inst. Mech. Eng.*, **160**, 224–232.

Fox, E. A., and V. E. Gex (1956). Single phase blending of liquids, *AIChE J.*, **2**, 539–544.

Galindo, E., and A. W. Nienow (1992). Mixing of highly viscous simulated xanthan fermentation broths with the Lightnin A315 impeller, *Biotechnol. Prog.*, **8**, 233–239.

Galindo, E., and A. W. Nienow (1993). The performance of the Scaba 6SRGT agitator in the mixing of simulated xanthan gum broths, *Chem. Eng. Technol.*, **16**, 102–108.

Grenville, R. K. (1992). Blending of viscous Newtonian and pseudo-plastic fluids, Ph.D. dissertation, Cranfield Institute of Technology, Cranfield, Bedfordshire, England.

Grenville, R. K., and J. N. Tilton (1996). A new theory improves the correlation of blend time data from turbulent jet mixed vessels, *Trans. Inst. Chem. Eng.*, **74**, 390–396.

Grenville, R. K., A. T. C. Mak, and S. W. Ruszkowski (1992). Blending of fluids in mixing tanks by re-circulating turbulent jets, *Proc. 1992 Institution of Chemical Engineers Research Event*, University of Manchester Institute of Science and Technology, Manchester, Lancashire, England, pp. 128–130.

Grenville, R. K., T. M. Hutchinson, and R. W. Higbee (2001). Optimisation of helical ribbon geometry for blending in the laminar regime, presented at MIXING XVIII, NAMF.

Hari-Prajitno, D., V. P. Mishra, K. Takenaka, W. Bujalski, A. W. Nienow, and J. McKemmie (1998). Gas–liquid mixing studies with multiple up- and down-pumping hydrofoil impellers: power characteristics and mixing time, *Can. J. Chem. Eng.*, **76**, 1056–1068.

Hirata, Y., A. W. Nienow, and I. P.T. Moore (1994). Estimation of cavern sizes in a shear-thinning plastic fluid agitated by a Rushton turbine based on LDA measurements, *J. Chem. Eng. Jpn.*, **27**, 235–237.

Hoogendoorn, C. J., and A. P. den Hartog (1967). Model studies on mixers in the viscous flow region, *Chem. Eng. Sci.*, **22**, 1689–1699.

Jaworski, Z., A. W. Pacek, and A. W Nienow (1994). On the flow close to cavern boundaries in yield stress fluids, *Chem. Eng. Sci.*, **49**, 3321–3324.

Johnson, R. T. (1967). Batch mixing of viscous liquids, *IEC Proc. Des. Dev.*, **6**, 340–345.

Khang, S. J., and O. Levenspiel (1976). New scale-up and design method for stirrer agitated batch mixing vessels, *Chem. Eng. Sci.*, **31**, 569–577.

Kramers, H., G. M. Baars, and W. H. Knoll (1953). A comparative study of the rate of mixing in stirred tanks, *Chem. Eng. Sci.*, **2**, 35–42.

Langheinrich, C., T. Eddleston, N. C. Stevenson, A. N. Emery, T. M. Clayton, N. K. H. Slater, and A. W. Nienow (1998). Liquid homogenisation studies in animal cell bioreactors of up to 8 m^3 in volume, *Food Bioprod. Process.* (*Trans. Inst. Chem. Eng. C*), **76**, 107–116.

Manikowski, M., S. Bodemeier, A. Lübbert, W. Bujalski, and A. W. Nienow (1994). Measurement of gas and liquid flows in stirred tank reactors with multiple agitators, *Can. J. Chem. Eng.*, **72**, 769–781.

Metzner, A. B., and R. E. Otto (1957). Agitation of non-Newtonian fluids, *AIChE J.*, **3**, 3–10.

Nagata, S., M. Nishikawa, H. Tada, and S. Gotoh (1971). Power consumption of mixing impellers in pseudo-plastic liquids, *J. Chem. Eng. Jpn.*, **4**, 72–76.

Nienow, A. W. (1997). On impeller circulation and mixing effectiveness in the turbulent flow regime, *Chem. Eng. Sci.*, **52**, 2557–2565.

Nienow, A. W., and T. P. Elson (1988). Aspects of mixing rheologically complex fluids, *Chem. Eng. Res. Des.*, **66**, 5–15.

Norwood, K. W., and A. B. Metzner (1960). Flow patterns and mixing rates in agitated vessels, *AIChE J.*, **6**, 432–437.

Okita, N., and Y. Oyama (1963). Mixing characteristics in jet mixing, *Jpn. Chem. Eng.*, **1**, 92–101.

Otomo, N., W. Bujalski, and A. W. Nienow (1993). Mixing time measurements for an aerated, single- and double-impeller stirred vessel by using a conductivity technique, *Proc. 1993 Institution of Chemical Engineers Research Event*, Birmingham, Jan., pp. 669–671.

Otomo, N., W. Bujalski, and A. W. Nienow (1995). An application of a compartment model to a vessel stirred with either dual radial or dual axial flow impellers, *Proc. 1995 Institution of Chemical Engineers Research Event*, Edinburgh, Jan. pp. 829–831.

Perry, R. H., and D. Green (eds.) (1984). *The Chemical Engineers' Handbook, 6th ed.*, Mcgraw-Hill, New York, Sec. 6.

Pollard, J., and T. A. Kantyka (1969). Heat transfer to agitated non-Newtonian fluids, *Trans. Inst. Chem. Eng.*, **47**, T21–T27.

Procházka, J., and J. Landau (1961). Studies on mixing: XII. Homogenisation of liquids in the turbulent regime, *Coll. Czech. Chem. Commun.*, **26**, 2961–2973.

Ràcz, I., and J. G. Wassink (1974). Strömungsverlauf und Mischzeiten in axialen Strahlmischern, *Chem. Ing. Tech.*, **46**, 261.

Rajaratnam, N. (1986). In *The Encyclopaedia of Fluid Mechanics*, Vol. 2, N. Cheremisnoff, ed., Gulf Publishing, Houston, TX, Chap. 15.

Rieger, F., V. Novák, and D. Havelková (1986). Homogenization efficiency of helical ribbon agitators, *Chem. Eng. J.*, **33**, 143–150.

Rieger, F., V. Novák, and D. Havelková (1988). The influence of the geometrical shape on the power requirements of ribbon impellers, *Int. Chem. Eng.*, **28**, 376–383.

Sano, Y., and H. Usui (1987). Effects of paddle dimensions and baffle conditions on the interrelations among discharge flow rate, mixing power and mixing time in mixing vessels, *J. Chem. Eng. Jpn.*, **20**, 399–404.

Shamlou, P. A., and M. F. Edwards (1985). Power consumption of helical ribbon mixers in viscous Newtonian and non-Newtonian fluids, *Chem. Eng. Sci.*, **40**, 1773–1781.

Solomon, J., A. W. Nienow, and G. W. Pace (1981). Flow patterns in agitated plastic and pseudo-plastic fluids, in *Fluid Mixing*, *Inst. Chem. Eng. Symp. Ser.*, **64**, A1–A13.

Van de Vusse, J. G. (1959). Vergleichende Rührversuche zum mischen löslicher Flüssigkeiten 12000 m^3 Behälter, *Chem. Ing. Tech.*, **31**, 583–587.

Vrabel, P., R. G. J. M. van der Lans, K. Ch. A. M. Luyben, L. A. Boon, and A. W. Nienow (2000). Mixing in large scale vessels stirred with multiple radial or radial and axial up-pumping impellers: modelling and measurements, *Chem. Eng. Sci.*, **55**, 5881–5896.

Wang, K., and S. Yu (1989). Heat transfer and power consumption of non-Newtonian fluids in agitated vessels, *Chem. Eng. Sci.*, **44**, 33–40.

Wichterle, K., and O. Wein (1981). Threshold of mixing non-Newtonian fluids, *Int. Chem. Eng.*, **21**, 116–120.

Wichterle, K., M. Kadlec, L. Žák, and P. Mitchka (1984). Shear rates on turbine impeller blades, *Chem. Eng. Commun.*, **26**, 25–32.

Zlokarnik (1967). Eigung von Rühren zum homogenisieren von Flüssigkeitenmischen, *Chem. Ing. Tech.*, **39**(9/10), 539–548.

CHAPTER 10

Solid–Liquid Mixing

VICTOR A. ATIEMO-OBENG

The Dow Chemical Company

W. ROY PENNEY

University of Arkansas

PIERO ARMENANTE

New Jersey Institute of Technology

10-1 INTRODUCTION

In this chapter the focus is on mixing operations involving, primarily, solid and liquid phases carried out in agitated or stirred vessels. Fundamental aspects of the hydrodynamics and mass transfer as well as practical design issues for solid–liquid mixing of both settling and floating solids in ungassed or gassed suspensions are discussed. Settling solid particles have a higher density than the liquid and will settle without agitation. Solids that float without agitation include solids that are less dense than the liquid, dense solids with trapped gas, and solids that are difficult to wet. Often, solid–liquid mixing operations are carried out in the presence of gas bubbles. These are known as *gassed suspensions*, in contrast to ungassed suspensions in the absence of gas bubbles. The gas bubbles may be introduced, directly as in solid-catalyzed hydrogenation reactions, entrained inadvertently or deliberately from the headspace, or evolved as in an evaporative crystallization or as a gaseous reaction product.

Solid suspensions are typically carried out in mechanically agitated or stirred vessels. Pumped liquid jets have also been used to suspend low concentrations of relatively slow settling solids. Although static mixers have been used to disperse fine solids into polymers, application of the technology is limited and beyond the scope of the present discussion.

Handbook of Industrial Mixing: Science and Practice, Edited by Edward L. Paul, Victor A. Atiemo-Obeng, and Suzanne M. Kresta
ISBN 0-471-26919-0

Not included in this chapter are several solid–liquid contacting operations, such as:

1. Dispersion of very fine particles in liquids where interfacial phenomena dominate both the dispersion process and the rheology of the suspension. An application of this technology is in the preparation of a stable solid suspension such as an agricultural "flowable" formulation by the addition of suspending aids, stabilizers, and so on. The book by Parfitt (1973) discusses this technology.
2. Liquid or gas fluidized beds.
3. Liquid–solid contacting in fixed bed systems.
   Froment and Bischoff (1990) discuss both fixed bed and fluidized bed systems.

10-1.1 Scope of Solid–Liquid Mixing

The primary objectives of solid–liquid mixing are to create and maintain a slurry and/or to promote and enhance the rate of mass transfer between the solid and liquid phases. The mixing operation promotes the

- Suspension of solids
- Resuspension of settled solids
- Incorporation of floating solids
- Dispersion of solid aggregates or control of particle size from the action of fluid shear as well as any abrasion due to particle–particle and impeller–particle impacts
- Mass transfer across the solid–liquid interface

10-1.2 Unit Operations Involving Solid–Liquid Mixing

Solid–liquid mixing is a key aspect of common unit operations in the chemical industry, including:

1. Dispersion of solids
2. Dissolution and leaching
3. Crystallization and precipitation
4. Adsorption, desorption, and ion exchange
5. Solid-catalyzed reaction
6. Suspension polymerization

These unit operations, with the exception of dispersion, involve mass transfer between the solid and liquid phases.

Dispersion of solids is a physical process where solid particles or aggregates are suspended and dispersed by the action of an agitator in a fluid to achieve a

uniform suspension or slurry. Applications include the preparation of a slurry of solid reactants or catalyst to feed a reactor as well as dispersion of solid pigments and other materials into a liquid.

Dissolution is a mass transfer unit operation during which the solid particle decreases in size and ultimately disappears as it is incorporated as solute in the liquid. In *leaching*, a soluble component of the solid dissolves, usually leaving a particle of different size, density, and/or porosity. For some rubber or plastic materials, the particles may actually swell initially. The density and viscosity of the resulting liquid may differ considerably from the original liquid for some systems. The process goal here is to achieve the desired rate of dissolution or leaching by agitation.

Crystallization and *precipitation* start with a solid-free liquid phase if unseeded. The solid particles form during the crystallization or precipitation operation. The solids grow in size as well as in population. The viscosity and density of the slurry thus formed usually increase. The process goals include control of the rate of nucleation and growth of the particles as well as the minimization of particle breakage or attrition. Both the average size and the particle size distribution are important properties. Liquid-phase mixing to achieve uniformity of supersaturation or to avoid local high concentration regions is important in achieving particle size control. Crystallization is discussed further in Chapter 17.

In *adsorption*, *desorption*, and *ion exchange*, there is mass transfer between the solid and the solution. Mass transfer is from the liquid phase into the solid in adsorption and from the solid into the liquid phase for desorption. In ion-exchange operations there is an exchange of ions between the solid and the liquid.

Solid-catalyzed reactions usually involve adsorption of reactants onto the surfaces of the catalyst particles where the reactions take place, followed by the desorption of the reaction products from the surface. A uniform suspension of catalyst particles ensures a uniform concentration of reactants and reaction products throughout the vessel. In addition, agitation reduces the diffusional mass transfer boundary layer, thus enhancing the solid–liquid mass transfer.

Suspension polymerization starts with the creation of a stabilized dispersion of monomer droplets. As polymerization proceeds, the monomer droplets polymerize, usually passing through a sticky phase. The protective coating of suspending agents (surfactants, etc.) and agitation conditions keep the droplets from coalescing. They also control particle size and size distribution. The mixing objective here is to produce and maintain, by agitation, a dispersion of uniform size drops and suspension of both monomer drops and eventually, polymer particles. The dispersion of monomer droplets and emulsion polymerization is discussed further in Chapter 12.

10-1.3 Process Considerations for Solid–Liquid Mixing Operations

The desired process results for solid–liquid mixing vary from process to process as indicated above in the brief discussion of several unit operations. It is the

responsibility of the process researcher and/or process engineer to determine the pertinent and specific process needs. Sometimes, results associated with other mixing operations—blending, gas–liquid, liquid–liquid, heat transfer, and so on—may be more important. Therefore, it is essential to consider and understand, early in the process development stage, all the physical and chemical phenomena necessary to achieve the desired process results. In particular, how these phenomena are influenced by the process chemistry, the properties of the solid and liquid phases, and the operational variables of mixing must be understood. The key considerations include the:

1. *Mode of process operations:* batch, semibatch [continuous addition to batch (con-add)], or continuous
2. Phases—solid, liquid, and/or gas phases—that are present or occur from the beginning to the end of the process
3. Properties of the solid and liquid phases, including stickiness and tendency to agglomerate
4. Unit operations involved from the beginning to the end of the process
5. Vessel geometry and internals
6. *Mixing parameters:* local or average fluid velocity or flow, local or average shear rates, blend time, power input, and so on.

10-1.3.1 Key Process Questions for Solid–Liquid Mixing. For each mixing operation, several key process-related issues must be addressed before scale-up and design. For solid–liquid mixing operations, key process questions include the following.

- *What is the process mode of operation: batch, semibatch, or continuous?* Whether a process is best run as a batch, semibatch, or continuous operation depends on the unit operation, upstream and/or downstream operations, and the volume of materials processed. For example, in a single stirred tank, a solid–liquid mixing operation requiring complete solid dissolution or complete reaction of the solid must, of necessity, be batch or semibatch. The solid–liquid mixing operations where a slurry is the end product can be batch, semibatch or continuous. For batch operations, the mixing requirements often change during the batch as a result of changes in physical and chemical properties and/or changes in the mixing volume for semibatch operations. It is therefore important to determine all the physical and chemical phenomena taking place during the entire duration of the batch. For continuous operations, the physical and chemical phenomena occurring during startup and shutdown must also be determined.
- *What phases are present or occur during the process?* The type of mixing operation to study, and the degree of difficulty in achieving the desired process result, depend on the phases present. The presence of solid and liquid phases only suggests that the mixing problem of interest is one of

solid–liquid mixing operation. For example, the mixing problem is blending rather than solid–liquid mixing if the settling velocity is less than about 0.5 ft/min or 0.0025 m/s. This condition occurs if the viscosity of the suspending liquid is very high, the solid particles are so small, and/or the density difference between the solid particle and the liquid is small. The presence of gas bubbles and/or immiscible liquids can significantly influence the ability to suspend the solids.

- *Is there a chemical reaction of the solid with the liquid?* Solid–liquid mixing operations involving chemical reactions often require a high relative velocity between the solid particle and the liquid—high local shear rate or agitation intensity—to minimize the thickness of the boundary layer for mass transfer. This is also true for the dissolution of a sparingly soluble solid, as discussed further in Chapter 13.
- *What are the physical properties of the solid and liquid phases present?* The degree of difficulty in solid suspension depends on several properties of the fluid and solid particles discussed in Section 10-2. The properties of interest include the relative density of the solid and liquid phases, the viscosity of the liquid, the wetting characteristics of the solid, the shape of the solid particles, and the mass or volume ratio of solids to liquid. Large and dense solids are more difficult to suspend than small light ones; spherical particles are also more difficult to suspend than thin flat disks. The impact of these properties on solid–liquid mixing must be studied and understood early in process research and development.
- *What degree or level of suspension is required?* The required degree or level of suspension depends on the desired process result and the unit operations involved. (Levels of suspension are discussed in Section 10-2.2.) For example, a higher degree of suspension is required in a crystallizer or slurry feed vessel than in a vessel for the dissolution of a highly soluble solid.
- *What is the minimum agitator speed to suspend the solids?* In stirred tanks, there is always an impeller speed below which settling solids will tend to accumulate on the bottom of the vessel. This speed is different for different types of impellers and for identical impellers located at different clearances from the bottom of the vessel. It also depends on the properties of the solid and liquid phases. The minimum speed may be estimated for certain impeller and tank geometries using the Zwietering correlation. It is advisable, however, to determine this value experimentally for processes where solid–liquid mixing is deemed critical. See Section 10-2.2 for details.
- *What happens to the suspension when agitation is decreased or interrupted?* Obviously, solids will settle or float depending on the properties of the solid relative to the liquid phase. The more important issues are whether the solids agglomerate and/or cake as they settle or how easy it is to resuspend them when agitation is increased or restored. This information is crucial for the proper mechanical design as well as instrumentation and control of the agitation. See Sections 10-2.2 and 10-5.9.

- *What happens to the suspension when agitation is increased?* Most solid–liquid mixing operations operate above the minimum speed for suspension. A higher agitation speed improves the degree of suspension and enhances mass transfer rates. The higher speed also translates into higher turbulence as well as local and average shear rates, which for some processes may cause undesirable particle attrition. Obviously, there is also a practical economic limit on the maximum speed of agitation.
- *What effect does vessel geometry have on the process?* The geometry of the vessel, in particular the shape of the vessel base, affects the location of dead zones or regions where solids tend to congregate. It also influences the minimum agitation speed required to suspend all particles from the bottom of the vessel. In flat-bottomed vessels, dead zones and thus "fillet formation" tend to occur in the corner between the tank base and the tank wall, whereas in dished heads the solids tend to settle beneath the impeller or midway between the center and the periphery of the base. The minimum agitation speed is typically 10 to 20% higher in a flat-bottomed vessel than in one with a dished head. Both the minimum agitation speed and the extent of fillet formation are also a function of impeller type, ratio of impeller diameter to tank diameter, and location of the impeller from the vessel bottom. In general, a dished-head vessel is preferred to a flat-bottomed vessel for solid–liquid mixing operations. There is little or no difference between ASME dished, elliptical, or even hemispherical dished heads as far as solid–liquid mixing is concerned. However, elliptical heads are preferred for higher-pressure applications.
- *What is the appropriate material of construction for the process vessel?* The main issue here is that, for steel or alloy vessels, the standard four wall-mounted baffles provide a better environment for solid–liquid mixing. The standard glass-lined vessels are usually underbaffled because of a deficiency of nozzles from which to mount baffles.

10-2 HYDRODYNAMICS OF SOLID SUSPENSION AND DISTRIBUTION

Solid suspension requires the input of mechanical energy into the fluid–solid system by some mode of agitation. The input energy creates a turbulent flow field in which solid particles are lifted from the vessel base and subsequently dispersed and distributed throughout the liquid. Nienow (1985) discusses in some detail the complex hydrodynamic interactions between solid particles and the fluid in mechanically agitated vessels. Recent measurements (Guiraud et al., 1997; Pettersson and Rasmuson, 1998) of the 3D velocity of both the fluid and the suspension confirm the complexity.

Solids pickup from the vessel base is achieved by a combination of the drag and lift forces of the moving fluid on the solid particles and the bursts of turbulent eddies originating from the bulk flow in the vessel. This is clearly evident in

Figure 10-1 Sudden pickup of solids by turbulent burst (Cleaver and Yates, 1973).

visual observations of agitated solid suspensions as in the video clip included on the accompanying CD ROM. Solids settled at the vessel base mostly swirl and roll around there, but occasionally, particles are suddenly and intermittently lifted up as a tornado might lift an object from the ground. An illustration of sudden pickup by turbulent bursts is shown in Figure 10-1.

The distribution and magnitude of the mean fluid velocities and large anisotropic turbulent eddies generated by a given agitator determine to what degree solid suspension may be achieved. Thus, different agitator designs achieve different degrees of suspensions at similar energy input. Also for any given impeller the degree of suspension will vary with D/T as well as C/T at constant power input. One of the video clips on the accompanying CD ROM shows the effect of D/T on solid suspension for a pitched blade impeller at constant power input.

For small solid particles whose density is approximately equal to that of the liquid, once suspended they continue to move with the liquid. The suspension behaves like a single-phase liquid at low solid concentrations; the mixing operation is more like blending than solid suspension. For heavier solid particles, their velocities will be different from that of the liquid. The drag force on the particles caused by the liquid motion must be sufficient and directed upward to counteract the tendency of the particles to settle by the action of gravity.

The properties of both the liquid and the solid particles influence the fluid–particle hydrodynamics and thus the suspension. Also important are vessel geometry and agitation parameters. The important fluid and solid properties and operational parameters include:

1. Physical properties of the liquid, such as:
   a. Liquid density, ρ_l (lb/ft^3 or kg/m^3)
   b. Density difference, $\rho_s - \rho_l$ (lb/ft^3 or kg/m^3)
   c. Liquid viscosity, μ_l (cP or $Pa \cdot s$)
2. Physical properties of the solid, such as:
   a. Solid density, ρ_s (lb/ft^3 or kg/m^3)
   b. Particle size, d_p (ft or m)

   c. Particle shape or sphericity, ψ (dimensionless factor defined by the ratio of surface area of a spherical particle of the same volume to that of a nonspherical particle)
   d. Wetting characteristics of the solid
   e. Tendency to entrap air or headspace gas
   f. Agglomerating tendencies of the solid
   g. Hardness and friability characteristics of the solid
3. Process operating conditions, such as:
   a. Liquid depth in vessel, Z (ft or m)
   b. Solids concentration, X (lb solid/lb liquid or kg solid/kg liquid)
   c. Volume fraction of solid, ϕ
   d. Presence or absence of gas bubbles
4. Geometric parameters, such as:
   a. Vessel diameter, T (ft or m)
   b. Bottom head geometry: flat, dished, or cone-shaped
   c. Impeller type and geometry
   d. Impeller diameter, D (ft or m)
   e. Impeller clearance from the bottom of the vessel, C (ft or m)
   f. Liquid coverage above the impeller, CV (ft or m)
   g. Baffle type and geometry and number of baffles
5 Agitation conditions, such as:
   a. Impeller speed, N (rps)
   b. Impeller power, P (hp or W)
   c. Impeller tip speed (ft/s or m/s)
   d. Level of suspension achieved
   e. Liquid flow pattern
   f. Distribution of turbulence intensity in the vessel

10-2.1 Settling Velocity and Drag Coefficient

A dense solid particle placed in a quiescent fluid will accelerate to a steady-state settling velocity. This velocity, often called the *free* or *still-fluid settling velocity*, occurs when the drag force balances the buoyancy and gravitational force of the fluid on the particle. In an agitated solid suspension, because of the complex turbulent hydrodynamic field, including solid–solid interactions, it is difficult to clearly define and/or measure a particle settling velocity. However, the particle settling velocity in an agitated solid suspension is a function of the free settling velocity and is always less than the free settling velocity (Guiraud et al., 1997).

The magnitude of the free settling velocity has proven useful in characterizing solid suspension problems into easy, moderate, or difficult categories (see Table 10-2). It is also used in solid–liquid mixing correlations, as described below.

Correlations for the free settling velocity have been derived for spherical particles. In Newtonian fluids, the free settling velocity, V_t, is calculated by the expression (Perry and Green, 1984).

$$V_t = \left(\frac{4 g_c d_p (\rho_s - \rho_l)}{3 C_D \rho_l} \right)^{1/2} \tag{10-1}$$

where g_c is the gravitational constant (32.17 ft/sec^2 or 9.81 m/s^2) and the drag coefficient, C_D, is a function of the particle Reynolds number, Re_p, and particle shape (see Figure 10-2):

$$Re_p = \frac{\rho_l V_t d_p}{\mu} \tag{10-2}$$

In Figure 10-2, the flow is assumed normal to the flat side of the disk and normal to the axis of the cylinder. The cylinder is assumed to have an "infinite" aspect ratio—length/diameter ratio.

The correlation for C_D (like the friction factor and the impeller power number, N_p) covers several hydrodynamic regimes. The corresponding ranges for Re_p and the correlating expression for C_D are shown in Table 10-1 for three hydrodynamic regimes.

When the expressions for C_D are substituted in eq. (10-1), the resulting expressions for the free settling velocity, V_t are, respectively:

- For the Stokes' law (laminar) regime, $Re_p < 0.3$:

$$V_t = \frac{g_c d_p^2 (\rho_s - \rho_l)}{18 \mu} \tag{10-3}$$

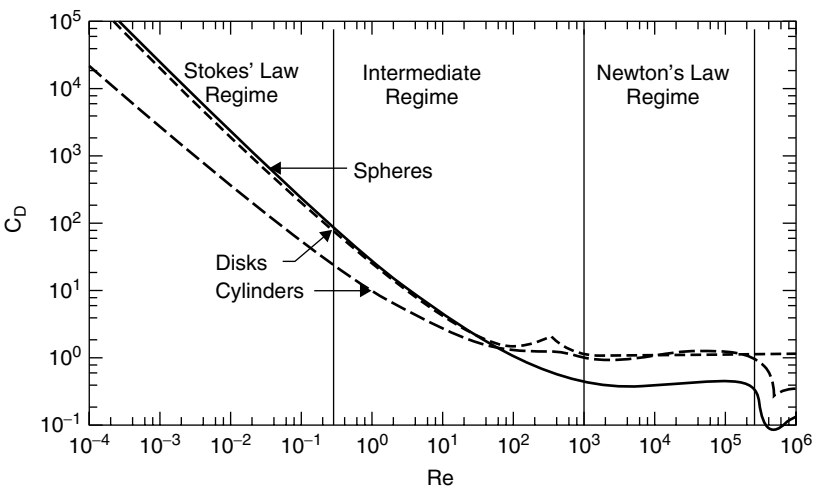

Figure 10-2 Drag coefficient as a function of Reynolds number.

Table 10-1 Hydrodynamic Regimes for Settling Particles

Regime	Reynolds Number	C_D Expression
Stokes' law (laminar)	$Re_p < 0.3$	$C_D = 24/Re_p$
Intermediate law	$0.3 < Re_p < 1000$	$C_D = 18.5/Re_p^{3/5}$
Newton's law (turbulent)	$1000 < Re_p < 35 \times 10^4$	$C_D = 0.445$

- For the Newton's law (turbulent) regime, $1000 < Re_p < 35 \times 10^4$:

$$V_t = 1.73 \left[\frac{g_c d_p (\rho_s - \rho_l)}{\rho_l} \right]^{1/2} \tag{10-4}$$

Figure 10-3 is a chart for estimating the free settling velocity for particles settling in water at ambient conditions.

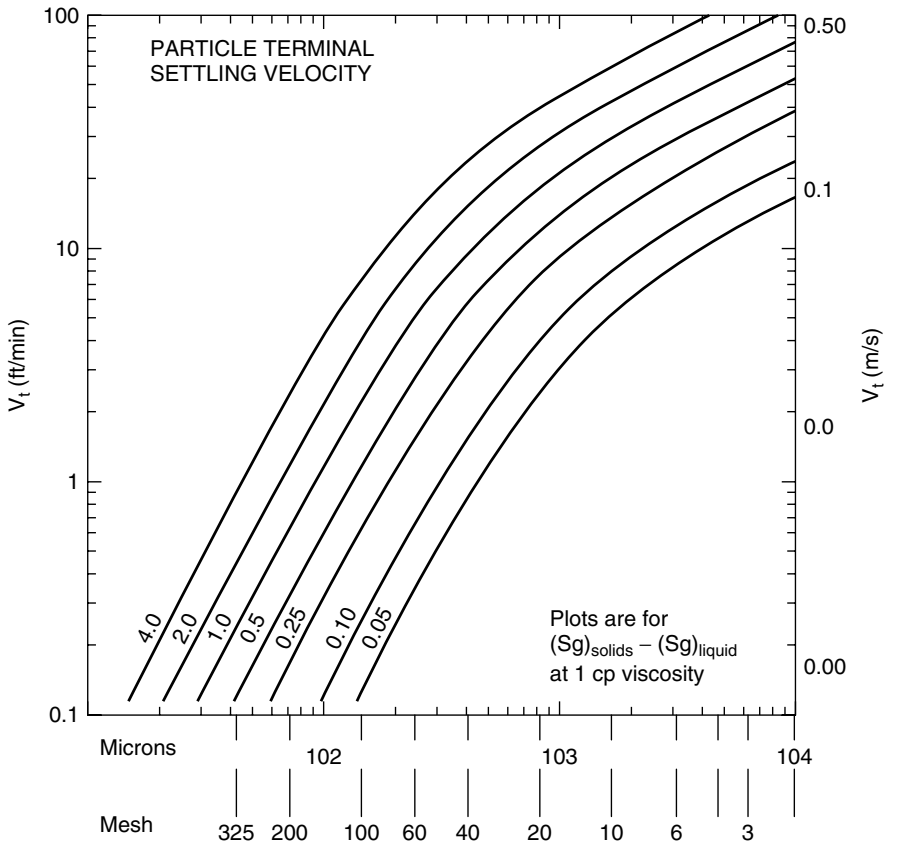

Figure 10-3 Free settling velocity, V_t, as a function of particle size and density difference.

10-2.1.1 Effect of Solids Particle Size and Distribution. Solids particles encountered in industrial applications usually have a distribution of sizes. Larger particles settle faster than smaller ones. Studies by Baldi et al. (1978) suggest that for a distribution of particle sizes, the appropriate particle diameter to use in the expressions above is the mass-mean diameter, $(d_p)_{43}$. This is calculated from size distribution data by

$$(d_p)_{43} = \frac{\sum_{i=1}^{N} n_i d_i^4}{\sum_{i=1}^{N} n_i d_i^3} \tag{10-5}$$

where d_i is the mean particle diameter of the ith size class and n_i is the number of particles in the ith size class. The value of n_i is calculated from the weight percent data by the expression

$$n_i = \frac{\text{mass of solids in the ith size class}}{\text{mass of particle of diameter } d_i}$$

However, in practice, the process engineer selects the largest particle size that must be suspended to achieve the desired process result.

10-2.1.2 Effect of Particle Shape and Orientation to Flow. As indicated by Figure 10-2, the shape of the particle, and particularly its orientation to flow, affects the settling velocity. Particle shape is often quantified by the sphericity, ψ, which is the ratio of the surface area of a spherical particle of the same volume to that of the nonspherical particle. Chapman et al. (1983) reported that for particles with sphericity between 0.7 and 1, it is sufficient to use eqs (10-3) and (10-4) and replace the particle diameter, d_p, with the diameter of a sphere of equal volume. For particles with sphericity less than 0.7, the estimation of the settling velocity is complicated by the fact that the orientation to flow is a function of the Reynolds number. The effect of shape on the settling of such particles must be evaluated experimentally. Correlations presented by Pettyjohn (1948) and Becker (1959) are recommended only for preliminary estimates.

10-2.1.3 Effect of Solids Concentration. The settling velocity expression above is based on the hydrodynamics of a single settling particle. The presence of other particles lowers the value of V_t. *Hindered settling* occurs because of the (1) interactions with surrounding particles, (2) interactions with the upward flow of fluid created by the downward settling of particles, and (3) increase in the apparent suspension viscosity and density. An empirical correlation for hindered settling in monodispersed suspensions is reported by Maude (1958) as

$$V_{ts} = V_t(1 - \chi)^n \tag{10-6}$$

where V_{ts} is the hindered settling velocity, V_t the free settling velocity, χ the volume fraction of solids in the suspension, and n is a function of the particle

Reynolds number, Re_p, as follows: $n = 4.65$ for $Re_p < 0.3$, $n = 4.375\ Re_p^{-0.0875}$ for $0.3 < Re_p < 1000$, and $n = 2.33$ for $Re_p > 1000$. This expression is recommended for preliminary estimates of the effect of solid concentration on the settling velocity. Davis and Gecol (1994) have reviewed hindered settling functions at low particle Reynolds numbers for mono- and poly-dispersed systems.

Example 10-1: Calculation of Settling Velocity. Calculate the free settling velocity for $AlCl_3$ crystals in methylene chloride using Figure 10-3 and also eqs (10-3) and (10-4). The solid and liquid properties are:

Particle size of $AlCl_3$ (d_p)	4–14 mesh (5000–1000 10^{-6} m)
Particle density of $AlCl_3$ (ρ_s)	2.44 g/mL (2440 kg/m^3)
Density of $MeCl_2$ (ρ_l)	1.326 g/mL at 20°C (1326 kg/m^3)
Viscosity of $MeCl_2$ (μ)	1 cP at 20°C (0.001 Pa · s or kg/m · s)

SOLUTION: Calculate $(\rho_s - \rho_l) = 2.44 - 1.326 = 1.114$ and read the value of the free settling velocity from Figure 10-3. The free settling velocity for the solids is approximately:

1. For particles of 5000 μm, $V_t = 55$ ft/min.
2. For particles of 1000 μm, $V_t = 22$ ft/min.

Note that using eqs. (10-3) and (10-4) require an iterative calculation since the value of the Reynolds number determines the flow regime and thus which equation to use. On the other hand, to evaluate the Reynolds number, one needs the value of V_t. Such problems are easily solved with an equation solver such as TK Solver software from Universal Technical Systems, Inc. or Microsoft Excel software.

1. For the Stokes' law (laminar) regime, $Re_p < 0.3$:

$$V_t = \frac{g_c d_p^2(\rho_s - \rho_l)}{18\mu} \tag{10-7}$$

$$V_t = \frac{9.81(5000 \times 10^{-6})^2(2.44 - 1.326)10^3}{18 \times 0.001}$$

$$= 15.2 \text{ m/s or } 49.8 \text{ ft/s or } 3000 \text{ ft/min} \qquad \text{which seems impractical}$$

Checking the particle Reynolds number, Re_p, yields

$$Re_p = \frac{\rho_l V_t d_p}{\mu} \tag{10-8}$$

$$= \frac{(1.326 \times 10^3 \text{ Kg/m}^3)(0.351 \text{ m/s})(5000 \times 10^{-6} \text{ m})}{0.001 \text{ kg/m} \cdot \text{s}}$$

$$= 100\ 776$$

The particle Reynolds number is outside the Stokes' law regime; therefore, we discard the calculated settling velocity.

2. For the Newton's law (turbulent) regime, $1000 < Re_p < 35 \times 10^4$:

$$V_t = 1.73\sqrt{\frac{g_c d_p(\rho_s - \rho_l)}{\rho_l}} \tag{10-9}$$

$$= 1.73\sqrt{\frac{9.81 \times 5000 \times 10^{-6}(2.44 - 1.326)}{1.326}}$$

$$= 0.35 \text{ m/s or } 1.15 \text{ ft/s or } 69 \text{ ft/min}$$

Checking the particle Reynolds number, Re_p, yields

$$Re_p = \frac{(1.326 \times 10^3 \text{ kg/m}^3)(0.351 \text{ m/s})(5000 \times 10^{-6} \text{ m})}{0.001 \text{ kg/m} \cdot \text{s}}$$

$$= 2327$$

Since this is within the Newton's law limits, we accept the velocity calculated.

Repeating the calculations for the 1000 μm particle size yields the following results:

1. For the Stokes' law (laminar) regime, $Re_p < 0.3$:

$$V_t = 0.608 \text{ m/s}$$

$$Re_p = 806$$

The particle Reynolds number is outside the Stokes' law limits; therefore, we discard the settling velocity calculated.

2. For the Newton's law (turbulent) regime, $1000 < Re_p < 35 \times 10^4$:

$$V_t = 0.157 \text{ m/s}$$

$$Re_p = 208$$

The particle Reynolds number is outside the Newton law limits, therefore, we discard the settling velocity calculated.

3. For the intermediate law regime, $0.3 < Re_p < 1000$:

$$V_t = 0.107 \text{ m/s or } 19.3 \text{ ft/min}$$

$$Re_p = 141.6$$

Since the particle Reynolds number is within the intermediate law limits, we accept the velocity calculated.

10-2.2 States of Solid Suspension and Distribution

In agitated vessels, the degree of solids suspension is generally classified into three levels: on-bottom motion, complete off-bottom suspension, and uniform suspension. These are illustrated in Figure 10-4.

10-2.2.1 On-Bottom Motion or Partial Suspension. This state is characterized by the visual observation of the complete motion of all particles around the bottom of the vessel. It excludes the formation of *fillets*, a loose aggregation of particles in corners or other parts of the tank bottom. Since particles are in constant contact with the base of the vessel, not all the surface area of particles is available for chemical reaction or mass or heat transfer. On-bottom motion conditions are sufficient for the dissolution of highly soluble solids.

10-2.2.2 Off-Bottom or Complete Suspension. The state of suspension known as off-bottom or complete suspension is characterized by the complete motion of all particles, with no particle remaining on the base of the vessel for more than 1 to 2 s. This condition is known as the *Zwietering criterion*. Under this condition, the maximum surface area of the particles is exposed to the fluid for chemical reaction or mass or heat transfer. The "just suspended" condition refers to the minimum agitation conditions at which all particles attain complete suspension.

In mechanically agitated vessels, the minimum agitation speed for the just suspended state, N_{js}, has been the subject of many experimental and theoretical analyses (Nienow, 1985). The pioneering study by Zwietering (1958) covered by far the widest range variables. The resulting correlation is discussed below.

10-2.2.3 Uniform Suspension. Uniform suspension corresponds to the state of suspension at which particle concentration and particle size distribution are practically uniform throughout the vessel; any further increase in agitation speed or power does not appreciably enhance the solids distribution in the fluid. A

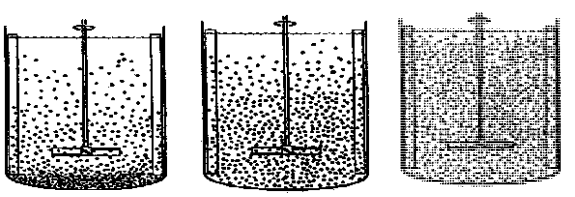

Figure 10-4 Degrees of suspension. (*a*) Partial suspension: some solids rest on the bottom of the tank for short periods; useful condition only for dissolution of very soluble solids. (*b*) Complete suspension: all solids are off the bottom of the vessel; minimum desired condition for most solid–liquid systems. (*c*) Uniform suspension: solids suspended uniformly throughout the vessel; required condition for crystallization, solid catalyzed reaction. See Visual Mixing CD affixed to the back cover of the book for several illustrative videos.

Table 10-2 Impact of Desired Result on Mixer Design[a]

		Power Ratio at Settling Velocity (ft/min)		
Suspension Criteria	Speed Ratio	16–60 Difficult	4–8 Moderate	0.1–0.6 Easy
On-bottom motion	1	1	1	1
Complete off-bottom suspension	1.7	5	3	2
Total uniformity	2.9	25	9	4

Source: Oldshue (1983).
[a]Power and speed depend on mixing criteria and settling velocity.

coefficient of variation of the solid concentration of about 0.05, or a uniformity of 95%, is often considered adequate for most process applications. A uniformity of 100% is impractical because there is always a fluid layer a few inches thick at the surface where particle concentration is lower because the axial lift velocity is small near the fluid surface.

Uniform suspension is often the desired process result for process operations where a representative sample of solids is required or a uniform concentration of solids must be achieved. For example, in crystallization, nonuniform solids concentration may lead to unacceptably high local supersaturation levels and subsequent nonuniformity in crystal growth. Also, in as practical a way as possible, a slurry must be fed at a uniform solids concentration to a continuous reactor or to a centrifuge for uniform buildup of solids required for proper filtration and washing of the solid cake.

As illustrated in Table 10-2, it requires increasing energy input to progress from on-bottom motion through complete suspension to the level of uniform suspension. For particles with a free settling velocity of 0.1 to 6.0 ft/min, the power required to achieve complete suspension and total uniformity is two and four times, to respectively, that required for on-bottom motion. For particles with a free settling velocity of 4 to 8 ft/min, the power ratios are 3 and 9 for complete suspension and total uniformity, respectively. For very fast settling particles, with a free settling velocity of 16 to 60 ft/min, the power ratios are 5 and 25 for complete suspension and total uniformity, respectively.

10-3 MEASUREMENTS AND CORRELATIONS FOR SOLID SUSPENSION AND DISTRIBUTION

Techniques for measuring the speed required for the condition for "just suspension" are discussed in Chapter 4 of this book and by Choudhury (1997). Also discussed are key aspects of the criteria, techniques, and precautions that one must take to obtain reliable data for solids suspension correlations. The Zwietering criterion of no particle remaining at the base of the vessel for more than 1 to 2 s is the basis for most of the published studies.

10-3.1 Just Suspended Speed in Stirred Tanks

There have been many experimental studies and theoretical analyses, with the pioneering work of Zwietering (1958) as the earliest known. He derived the following correlation from dimensional analysis and estimated the exponents by fitting to data for just suspended impeller speed, N_{js}:

$$Re_{imp}^{0.1}\ Fr^{0.45}\left(\frac{D}{d_p}\right)^{0.2} X^{0.13} = S \tag{10-10}$$

The correlation is often expressed in dimensional form as

$$N_{js} = S\nu^{0.1}\left[\frac{g_c(\rho_s - \rho_l)}{\rho_l}\right]^{0.45} X^{0.13} d_p^{0.2} D^{-0.85} \tag{10-11}$$

where Re_{imp} is the impeller Reynolds number, $Re_{imp} = N_{js}D^2/\nu$; Fr the Froude number, $Fr = \frac{[\rho_l]}{(\rho_s - \rho_l)} N_{js}^2 D/g_c$; D the impeller diameter (m); d_p the mass-mean particle diameter, $(d_p)_{43}$ (m); X the mass ratio of suspended solids to liquid × 100 (kg solid/kg liquid); S the dimensionless number which is a function of impeller type, as well as of D/T and C/T; N_{js} the impeller speed for "just suspended" (rps); ν the kinematic viscosity of the liquid (m^2/s); g_c the gravitational acceleration constant, 9.81 m/s^2; ρ_s and ρ_l the density of particle and the density of liquid (kg/m^3).

With the exception of the density difference, the influence of fluid and particle properties on N_{js} is not large, as indicated by the small exponents on the kinematic viscosity, ν, the particle diameter, d_p, and the solid loading parameter, X, in eq. (10-11). The density difference is the property with the largest influence on N_{js}. Its exponent reflects the effect of the terminal settling velocity of the particles. The exponent on the impeller diameter, D, represents the effect of scale. Note that an exponent of −0.67 on D would imply a scaling rule based on power per volume.

More recent studies (Nienow, 1968; Baldi et al., 1978; Rao et al., 1988; Mak, 1992; Choudhury, 1997) generally corroborate Zwietering's original findings. Choudhury (1997) has pointed out regions of interest where Zwietering's correlation is not as reliable. They include solids loading below 2 vol %, high d_p/T values, and high solids loading (greater than 15 vol %).

10-3.1.1 Effect of Fluid Viscosity. Most studies and applications of solid suspension occur in the turbulent regime, so the small effect of viscosity is expected. In fact, published values of the viscosity exponent range from 0 to 0.2 for experimental studies (Zwietering, 1958; Chapman et al., 1983; Ibrahim and Nienow, 1994; Rieger and Ditl, 1994). This suggests that the true hydrodynamic mechanism for the just suspended condition remains fuzzy. There may actually exist a hydrodynamic regime where there is little or no influence of viscosity and another where the influence is reflected in a positive value of the exponent.

The highest viscosity tested in the studies cited is only 100 mPa · s (Ibrahim and Nienow, 1994). What happens when the fluid viscosity is even higher remains to be determined. With a more viscous fluid, or as the transitional flow regime is approached, the hydrodynamics near the vessel base may change and make it more difficult for solids to be picked up, even though the bulk of the fluid remains turbulent.

10-3.1.2 Effect of Solid Loading. Zwietering chose to represent the effect of solid loading with the parameter X defined above. The exponent on this parameter fits experimental data reliably for values of X from about 5 to 170, which corresponds to about 2 to 40 vol% by volume for sand at a solid density of 2600 kg/m^3.

Choudhury (1997) and Choudhury et al. (1995) questioned the appropriateness of the use by Zwietering of the X parameter to correlate the effect of solid loading. They preferred the use of the volume fraction as a percent, %V, because a designer can specify it directly. The following expressions are useful for converting between various measures of solid loading in a slurry. To convert from volume percent, vol %, use

$$X = 100\frac{\rho_s \text{vol}\%}{\rho_l(100 - \text{vol}\%)}$$

In terms of weight percent of solids, wt%, the corresponding expression is

$$X = 100\frac{\text{wt}\%}{100 - \text{wt}\%}$$

When converting from slurry density, ρ_{av}, the expression is

$$X = 100\frac{M_s}{\rho_{av}V - M_s}$$

where V is the total slurry volume and M_s is the mass of solids.

10-3.1.3 Effect of Fluid Particle Size. Several studies (Zolfagharian, 1990; Choudhury et al., 1995; Choudhury, 1997) indicate that the effect of particle diameter is not as simple as the Zwietering correlation suggests, particularly at solid loading less than about 5 wt%. The exponent reported by Zwietering appears to be an average value for d_p between 0.20 and 1 mm. For particles greater than about 1 mm in diameter, N_{js} appears to be unaffected by the particle size. Choudhury reported this critical particle in terms of d_p/D at a value of about 0.01. On the other hand, for particles smaller than 0.20 mm, the average value of the exponent was about 0.5.

10-3.1.4 Effect of Vessel and Impeller Geometry and Scale. The effects of the geometry of the impeller, vessel, and its internals are subsumed in the

Table 10-3 Parameters for Solids Suspension in Dished Vessels

Impeller Geometry and Location	Zwietering Constant, S
A-310 (T/2.4)	
C = T/4	6.9
A-310 (T/2)	
C = T/4	7.1
30° PBT (T/3, D/2.5)	
C = T/4	6.4
C = T/6	7.1
C = T/8	7.2
45° PBT (T/3.3, D/2.1)	
C = T/4	4.5
C = T/8	4.3
45 PBT (T/3, D/3.5)	
C = T/4	4.8
C = T/6	4.6
C = T/8	4.2
45° PBT (T/2.5, D/2.8)	
C = T/4	4.7
C = T/8	3.4
45° PBT (T/2, D/3.5)	
C = T/4	5.2
C = T/6	4.2
C = T/8	3.7
45° PBT (T/2, D/6)	
C = T/4	5.5
C = T/8	
45° PBT (T/1.7, D/3.5)	
C = T/4	6.7
C = T/6	5.1
C = T/8	4.4
45° PBT (T/1.7, D/4.3)	
C = T/4	6.8
C = T/8	3.8
45° PBT (T/1.4, D/5.0)	
C = T/4	5.4
C = T/8	4.5
45° PBT (T/3, D/4)	
C = T/4	4.4
C = T/6	4.1
C = T/8	3.7
90° PBT (T/3, D/5)	
C = T/4	4.4
C = T/6	4.1
C = T/8	4.1

Source: Mak (1992).

S parameter. Representative values of the impeller-specific Zwietering constant, S, are listed in Table 10-3 for a variety of impellers. Note that the value of S varies with D/T and C/T. It is smaller at smaller C/T (i.e., an impeller mounted closer to the vessel bottom), and larger D/T (i.e., a larger-diameter impeller. Obviously, there are practical as well as performance limits on these dimensions. For example, it is clearly evident in the solid suspension video clip on the accompanying CD ROM that a large-diameter pitched blade turbine (D/T = 0.75) is poor at solid suspension because of the resulting flow patterns. When the power number of the impellers is taken into account, it becomes clear that axial flow impellers (e.g., Lightnin A-310, Chemineer HE-3) are able to achieve a just suspended state at a lower rotational speed than can a pitched blade or disk turbine. The resulting axial flow developed by high efficiency impellers is higher at the vessel base than for radial flow impellers. They are also more effective at higher clearances from the vessel base (i.e., larger values of C/T).

Zwietering provided plots of S as a function of D/T and C/T. Armenante et al. (1998) and others [see references cited in Armenante and Nagamine (1998)] have sought simple mathematical expressions to describe the effects of geometry (D/T and C/T) to facilitate the calculation of N_{js}. Their results are yet to be validated with data from large scale tests and for vessels with dished bottoms. Published data (Guerci et al., 1986) indicate that the just suspended condition is more easily achieved in dish-bottomed vessels than in flat-bottomed ones. Just suspension is impractical with conical bottoms.

It must be emphasized that studies of the minimum agitation speed for the just suspended state, N_{js}, address primarily hydrodynamic mechanisms associated with particle pickup from the vessel base and not necessarily the distribution of particles. Therefore, it is not expected that the use of multiple impellers would significantly affect N_{js}.

Example 10-2: Calculation of the Impeller Speed for Just Suspension. Calculate the just suspension impeller speed for suspending $AlCl_3$ crystals in methylene chloride. The solid and liquid properties are given in Example 10-1. Other data are as follows: Ratio of solid to liquid, X: 0.4. Kinematic viscosity of the liquid, ν: (0.001 kg/m · s)/1326 kg/m^3 or 7.541×10^{-7} m^2/s.

The impeller is a 45° pitched blade with a D/T value of 1/3 and blade width of D/4 located at C/T value of $\frac{1}{8}$ in a vessel with a diameter, T, of 48 in. The impeller diameter is 28.5 in. or 0.724 m; the S value from Table 10-3 is 3.7.

SOLUTION: We use the Zwietering correlation. For 5000 μm particles,

$$N_{js} = 3.7 \times (7.541 \times 10^{-7})^{0.1} \left[\frac{9.81(2.44 - 1.326)}{1.326}\right]^{0.45} \times 0.4^{0.13}(5 \times 10^{-3})^{0.2}(0.724^{-0.85})$$

$$= 0.95 \text{ rps or } 57 \text{ rpm}$$

For 1000 μm particles, use the fact that $N_{js} \propto d_p^{0.2}$, to obtain $N_{js} = 0.69$ rps or 41 rpm.

10-3.2 Cloud Height and Solids Distribution

In solid suspensions there is a distinct level to which most of the solids are lifted within the fluid even at speeds above N_{js}. The distance from the bottom of the vessel to this level is called the *cloud height*. The liquid below this height is solid-rich, while above it there is only an occasional visit by a few small solids. Hicks et al. (1993, 1997) and Bujalski et al. (1999) have reported extensive data on cloud height and solid distribution. Bujalski et al. (1999) also reported that the blending between the solid-rich and solid-free portions is rather poor, and can result in a blend time as much as 20 times longer in the solid-free region than in the solid-rich volume.

The data of Hicks et al. (1993) for single impellers showed that the cloud height increases with increasing impeller D/T at N_{js}. They reported a cloud height at N_{js} to be at about 70% of the slurry height for a single four-bladed 45° pitched blade turbine or a Chemineer HE-3 impeller with $D/T = 0.35$ located at $C/T = 0.25$ in a fluid with $Z/T = 1$. The cloud height was greater than 95% of the slurry height at impeller speeds of 1.5 times N_{js}. When the slurry height was increased to $Z/T = 1.75$, the cloud height was only about 40% of the slurry height at N_{js} and never got above 70%, even at three times N_{js}. They also reported that the cloud height improves with the addition of a second impeller. The best separation distance between impellers was three impeller diameters ($S/D = 3$). Bakker et al. (1994) showed that at this separation the dual impellers generate one large flow loop. However, when S/D is increased to 3.7, two separated flow loops are formed and the cloud height drops to the same level as for the single impeller.

Bittorf and Kresta (2002) have applied a wall jet model successfully to predict the cloud height data of Hicks et al. (1997) and Bujalski et al. (1999). The proposed model for purely axial impellers (i.e., A310 or HE3) is

$$CH = \frac{N}{N_{js}}\left[0.84 - 1.05\frac{C}{T} + 0.7\frac{(D/T)^2}{1-(D/T)^2}\right] \tag{10-12}$$

where CH is the cloud height made dimensionless with T. The model is good for $0.154 < D/T < 0.52$ for solids with a terminal settling velocity less than 0.143 m/s. The model agrees with the data of Hicks et al. (1993, 1997) and predicts that an impeller with a larger D/T located at small D/T results in a higher cloud height.

10-3.3 Suspension of Solids with Gas Dispersion

Three-phase (gas–liquid–solid) systems such as gaseous slurry reactions in stirred vessels are common in the chemical industry. They present special mixing challenges. The presence of gas tends to disturb the liquid flow patterns established

by the rotating impellers. Sometimes the gas is entrapped by solid agglomerates increasing their tendency to float. In general, laboratory or pilot testing is a must for reliable scale-up and design of three-phase slurry systems.

In a study of gassed solid suspension in an agitated vessel, Chapman (1981) found that for small-diameter ($D = T/4$) 45° pitched blade impellers, a sudden collapse of the suspension occurs at some critical gas rate. This is when the flow pattern becomes dominated by gas flow as opposed to impeller flow. The gas flow decreases the eddies and the upward velocities that maintain the suspension.

A theoretical correlation for N_{js} by Baldi et al. (1978) implies that N_{js} for gassed slurry systems is higher than for ungassed systems. This has been confirmed (Chapman et al., 1983) in experiments performed in 0.56 m-diameter vessels using particles of size greater than 80 mm and particle density greater than 1.2 g/cm^3 in distilled water. Chapman found that as the gas rate is increased, substantial increases in N_{js} are required to achieve a complete suspension of the solids. He also found that the impeller speed required for the just suspended state is always higher than that required for a complete dispersion of the gas bubbles. At low gas rates (volume of gas per minute per volume of liquid, vvm, less than 0.75), he found 45° pitched blade impellers to be more efficient than disk or Rushton turbines for solid suspension.

10-3.4 Suspension of Solids in Liquid-Jet Stirred Vessels

Jet mixers (see Chapter 9) are not normally used for solid suspension. However, it may be more economical to use liquid jets to suspend incidental solids in a vessel not initially intended for a solid–liquid mixing application. For example, a vessel designed normally for liquid storage may occasionally see sludge or solids accumulate from process upsets, including changes in concentration or temperature or failure of an upstream filter. It may be more difficult or expensive to retrofit such a vessel with a mechanical agitator than to install a jet mixer using the existing loading or unloading pump and piping system.

Shamlou and Zolfagharian (1990) have studied liquid-jet stirred suspension and found the mechanism of suspension to be similar to impeller-stirred suspension. The preferred design consists of a downward-pointing feeder nozzle centrally mounted with the tip fully submerged in the slurry. They found that to achieve an acceptable cloud height, the tip of the nozzle should be below half the slurry height. They showed also that:

1. There is no significant effect of the jet clearance—the distance between the tip of the jet and the vessel bottom—on the minimum jet velocity for solid suspension. The recommendation is to use the smallest practical jet clearance, but greater than eight jet nozzle diameters, to avoid erosion of the tank base.

2. The minimum jet velocity for off-bottom suspension, V_{js}, may be estimated using the following dimensional correlation:

$$V_{js} = 2\left(\frac{\rho_s - \rho_l}{\rho_l}\right)^{2.08} \frac{\nu^{0.16} g^{0.42} T^{1.16} d_p^{0.1} C_w^{0.24}}{D_j} \tag{10-13}$$

where V_{js} is the minimum jet velocity for off-bottom suspension or "just suspended" (m/s); d_p the mass-mean particle diameter, $(d_p)_{4,3}$ (m); C_w the percentage weight fraction of solids; D_j the jet diameter, (m). T the vessel diameter (m); It is worth noting the similarity between the proposed equation for V_{js} and the Zwietering correlation.

10-3.5 Dispersion of Floating Solids

Without adequate agitation, solid particles less dense than the liquid will float. Also, fine solids such as flour or powders may entrap large amounts of air, which reduces the effective density, causing them to float. Sometimes the solids are difficult to wet with the liquid and may form large clumps with entrapped air. Below is a brief summary of work reported in the open literature. This is offered as a guide but with the advise that in almost all cases, lab and pilot testing will be required for meaningful scale-up and design.

Studies using 10 wt% polyethylene in tap water and others using cork or polypropylene particles in water or corn syrup solutions (Joosten et al., 1977; Hemrajani et al., 1988; Thring, 1990; Siddiqui, 1993) indicate that formation of a controlled vortex is the key to achieving a complete dispersion and suspension of floating solids. The controlled vortex is obtained by using various partial baffles in the vessel rather than no baffles at all. All these studies indicate that dispersion of floating solids requires more energy than for settling solids.

The Froude number, N_{Fr}, is a predominant correlating parameter in these systems, where liquid surface behavior is so important. Joosten et al. (1977) have developed a correlation that has been used successfully to design a commercial mixing system for suspending floating solids in a 50 m^3 vessel. The correlation is

$$N_{Fr} = 3.6 \times 10^{-2}\left(\frac{D}{T}\right)^{-3.65}\left(\frac{\rho_l - \rho_s}{\rho_l}\right)^{0.42} \tag{10-14}$$

where

$$N_{Fr} = \frac{N^2 D}{g_c} \tag{10-15}$$

Joosten et al. (1977) recommend a down-pumping 45° pitched blade impeller in a vessel with a single baffle whose width is one-fifth the impeller diameter submerged to a depth of one-third the impeller diameter to produce a noncentral vortex. Hemrajani et al. (1988) recommend a down-pumping 45° pitched blade

impeller in a vessel with four baffles that are $\frac{1}{50}$ the tank diameter. Siddiqui also recommends a down-pumping 45° pitched blade impeller but in a vessel with three partially immersed standard baffles 90° apart immersed to different depths but with one or two of the baffles extending to the top impeller. Siddiqui (1993) found this design to be more effective than Hemrajani's for either standard vessels or for a tall vessel with a liquid height/tank diameter greater than 1.2. The variety of recommendations by these researchers is indicative of the complexities involved in suspending floating solids. Reliable scale-up and design will require careful experimental studies.

10-4 MASS TRANSFER IN AGITATED SOLID–LIQUID SYSTEMS

As noted earlier, with the exception of the purely physical process of producing a slurry, unit operations involving solid–liquid mixing are mass transfer processes. These include:

- Leaching
- Dissolution of solids with or without chemical reaction
- Precipitation
- Crystallization–nucleation and crystal growth
- Adsorption
- Desorption
- Ion exchange
- Solid-catalyzed reactions
- Suspension polymerization

Mass transfer between a solid and the liquid is discussed in great detail by Doraiswamy and Sharma (1984) and in other books devoted to a particular mass transfer operation, such as crystallization (Mullins, 1993). In the following sections we highlight several important aspects.

10-4.1 Mass Transfer Regimes in Mechanically Agitated Solid–Liquid Systems

In solid–liquid mass transfer processes, the rate-controlling steps are:

1. Diffusion in the liquid film surrounding the solid particles (film diffusion)
2. Diffusion within the particles—in pores or through the solid phase itself (particle diffusion), as in ion exchange
3. Chemical reaction at the surface of the particle (surface reaction)

Agitation affects only the film diffusion controlled process.

The rate of diffusional mass transfer, M, is defined as a product of the diffusional mass transfer coefficient, k_{SL}, the interfacial area for mass transfer, a_p, and the concentration driving force, $[A^*] - [A]$:

$$M = k_{SL} a_p ([A^*] - [A]) \tag{10-16}$$

The variables $[A^*]$ and $[A]$ are the concentration of the solid material, A, at the solid surface and in the bulk of the liquid, respectively. The interfacial area per unit volume is

$$a_p = 6\frac{\phi}{\rho_s d_p} \tag{10-17}$$

where ϕ is the solid loading with units of g/cm^3 solid-free liquid.

In a reactive diffusion system the dissolved solid undergoes a reaction in the bulk liquid or at the solid–liquid interface. The reaction rate may be expressed as a product of the reaction rate constant, k_r, and concentration to some power, n:

$$M = k_r [A]^n \tag{10-18}$$

The constants, k_{SL}, k_r, and n are to be determined from experimental data or from available correlations.

A key issue in solid–liquid reactions is determination of the controlling process regime: chemical reaction in the bulk liquid phase or mass transfer in the liquid film surrounding the solid particle. Experimentally, this is done by checking the effect of agitator speed on the observed process rate.

The controlling regime depends on the relative values of k_{SL} and k_r for first-order reactions as follows:

1. Chemical reaction controls when $k_r/k_{SL} \leq 0.001$.
2. Diffusional mass transfer controls when $k_r/k_{SL} \geq 100$.

For a reaction such as $A + B \rightarrow$ products, where A is the solid and B is a liquid phase reagent, Figure 10-5 shows schematically the concentration gradients for four different regimes that can occur: bulk reaction (regime 1), film diffusion (regime 2), film kinetics (regime 3), and instantaneous reaction (regime 4). Note that when the process is mass transfer controlled, there are three possible regimes (regimes 2, 3, or 4), depending on the kinetics of the reaction:

- In regime 1, as noted above, the reaction is so slow or the solubility of the solid is so high that the concentration of the solid species is essentially equal to the equilibrium conditions at the solid–liquid interface. Bulk liquid-phase reaction governs the overall process.
- In regime 2, the reaction is fast enough to keep the bulk liquid-phase concentration of the solid essentially zero but not fast enough to occur substantially

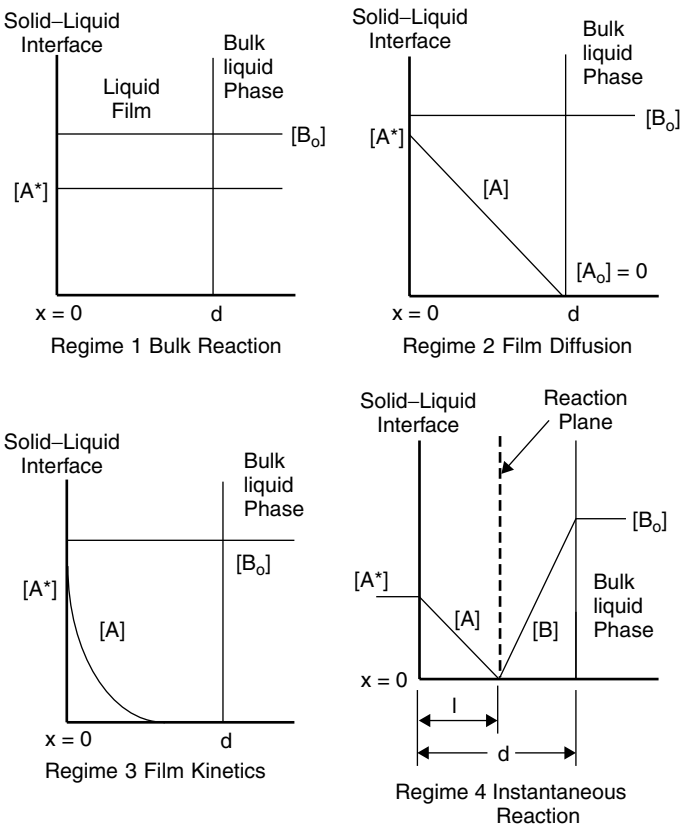

Figure 10-5 Schematic diagram of concentration gradients for solid–liquid reactions.

in the liquid film. There is no enhancement of mass transfer due to reaction. Diffusion and reaction take place in series.

- In regime 3, the reaction is sufficiently fast to consume the dissolved solid reactant completely in the liquid film. Diffusion and reaction occur simultaneously in a parallel fashion in the liquid film. The mass transfer coefficient has no effect on the overall process rate.
- In regime 4, the reaction is so fast (virtually instantaneous) that the reactant (A) and the liquid-phase reactant (B) cannot coexist. Diffusion of A from the solid–liquid interface and diffusion of B from the bulk liquid toward the reaction plane control the overall process.

Intermediate conditions between regimes are also possible. These correspond to cases where the concentration of species in the liquid film remains finite instead of going to zero. Doraiswamy and Sharma (1984) discuss these cases in some detail.

It is important to know the regime of a particular reaction system, since the equipment choice and the effect of design and operating variables on the process performance depend on the regime. A lack of this fundamental understanding leads to many apparent discrepancies between different scales of operations and sometimes to scale-up failures. For instance, in the lab the process may be operating in regime 1, while in production scale it could be in regime 2. Alternatively, one may design equipment for minimal mass transfer requirements based on the confirmation of regime 1 on lab scale only to find much lower process rates. The effect of temperature is minimal if the system is in regimes 2 and 4, substantial in regime 3 (apparent activation energy is half of the true activation energy), and maximum in regime 1 (apparent activation energy is equal to the true activation energy). Solid–liquid reactions are discussed further in Chapters 13 and 17.

10-4.2 Effect of Impeller Speed on Solid–Liquid Mass Transfer

Many authors (Nienow, 1975; Nienow and Miles, 1978; Chaudhari, 1980; Conti and Sicardi, 1982) have reported the effect of agitation on the diffusional mass transfer coefficient, $k_{SL}a_p$. It is sufficient to say that the diffusional mass transfer rate is affected primarily by the impact of agitation on the hydrodynamic environment near the surface of the particle, in particular the thickness of the diffusional boundary layer surrounding the solid. The hydrodynamic environment near the particle surface depends on the properties of the fluid properties as well as those of the particles. The specific variables were introduced in Section 10-2.1.1. In addition to these, the diffusivity, D_A, also influences the diffusional mass transfer.

The important hydrodynamic variables are the relative velocity, V_s, between the solids and the liquid (also know as *slip velocity*) and the rate of renewal of the liquid layer near the solid surface. The relative velocity, V_s, obviously varies from point to point within the vessel, and the average value is difficult to estimate. So, in practice, the relative velocity, V_s, is assumed equal to the free settling velocity, V_t. The renewal of the boundary layer depends on the intensity of turbulence around the solid particle as well as the convective velocity distribution in the vessel.

The observed effect of agitation is depicted in Figure 10-6. As the stirrer speed increases, the volumetric mass transfer coefficient, $k_{SL}a_p$, increases. If the process is mass transfer controlled, the observed rate of reaction increases with increasing impeller speed. However, beyond the just suspended or complete suspension state the observed rate may not increase much with increasing rpm or mixing intensity, indicating that the overall process is bulk reaction controlled. For extremely slow reactions of highly soluble solids, on-bottom motion to prevent stagnant pockets may be all that is needed.

In general, the specific impact of agitation must be determined experimentally for each system. The correlations discussed below are presented to provide a guide and insight into the expected effects of various variables on solid–liquid mass transfer.

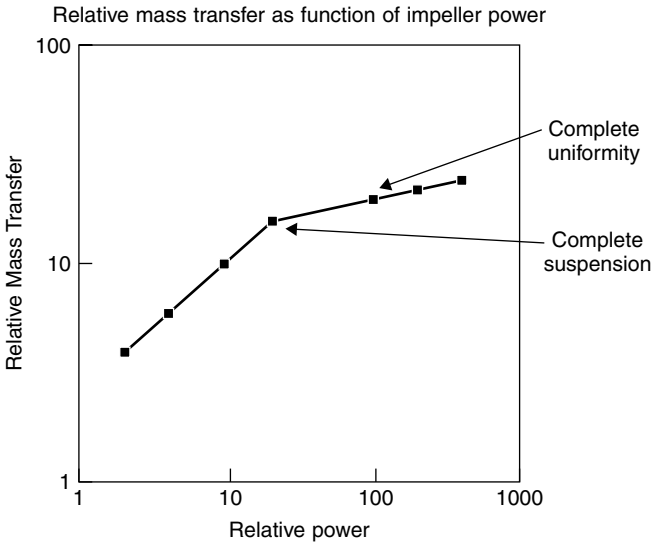

Figure 10-6 The mass transfer increases sharply up to the point of complete suspension and at a much lower rate to complete uniformity.

10-4.3 Correlations for the Solid–Liquid Mass Transfer

Several correlations for k_{SL} have been reported in the literature. The Froessling type equation developed by Nienow and Miles (1978) based on the theory of slip velocity between the liquid and solid particles: namely,

$$Sh = 2 + 0.44Re_p^{1/2}Sc^{0.38} \tag{10-19}$$

has proven useful for estimating k_{SL} or establishing the effect of solid and fluid properties as well as agitation parameters. In this equation, the Sherwood number, Sh, the particle Reynolds number, Re_p, and the Schmidt number, Sc, are defined in terms of the particle diameter, d_p, the liquid density, ρ_l, liquid viscosity, μ_l, terminal velocity, V_t, and diffusivity, D_A, as

$$Sh = \frac{k_{SL}d_p}{D_A} \tag{10-20}$$

$$Re_p = \frac{\rho_l V_t d_p}{\mu_l} \tag{10-21}$$

$$Sc = \frac{\mu_l}{\rho_l D_A} \tag{10-22}$$

The Froessling correlation is not applicable to solid–liquid systems where the settling velocity or slip velocity is small, $\ll 0.1$ ft/min or 0.0005 m/s. Figure 10-3 can be used to estimate the combination of the range of particle sizes and density

difference, $(\rho_s - \rho_l)$ that lead to small values of the settling velocity. For such systems, the correlation

$$Sh = 2 + 0.47 Re_p^{0.62} Sc^{0.36} \left(\frac{D}{T}\right)^{0.17} \tag{10-23}$$

developed by Levins and Glastonbury (1972a,b), based on Kolmogoroff's theory of isotropic turbulence, is recommended (Nienow, 1975). (See Chapter 2 for a discussion of isotropic turbulence.) In this correlation the particle Reynolds number, Re_p, is defined in terms of the power input per unit mass of solid, ε_p, as follows:

$$Re_p = \frac{\rho_l \varepsilon_p^{1/3} d_p^{4/3}}{\mu_l} \tag{10-24}$$

Key Points

1. Experiments show that the measured value of k_{SL} can be significantly different from that estimated with the correlations above (Nienow, 1975). Therefore, for reliable scale-up or design, laboratory- or pilot-plant experimentation to measure the rate of mass transfer is a must for systems where mass transfer is important.
2. Experiments indicate that solid–liquid mass transfer rate increases relatively rapidly with increasing impeller speeds up to the just suspended state, N_{js}. This is a result of increases in both the interfacial area per volume, a_p, and the mass transfer coefficient, k_{SL}. Beyond N_{js}, a_p is independent of agitation because all the solid surface available for mass transfer is now exposed, but the mass transfer coefficient, k_{SL}, continues to increase, although at a much lower rate. The overall effect is illustrated in Figure 10-6.
3. At impeller speeds corresponding to N_{js}, the value of k_{SL} is independent of the geometry of the vessel, impeller design, or the specific power consumption (Doraiswamy and Sharma 1984).
4. The functional relationship between k_{SL} and the speed of agitation depends on the hydrodynamic regime of agitation. In the turbulent regime, where the impeller Reynolds number is greater than 1000, the value of k_{SL} is independent of particle size and practically independent of the density difference (Doraiswamy and Sharma, 1984).
5. At impeller speeds near N_{js}, the value of k_{SL} will be a strong function of the density difference between the particle and the liquid (Doraiswamy and Sharma, 1984).

Example 10-3: Calculation of Solid–Liquid Mass Transfer Coefficient. (Adapted from Doraiswamy and Sharma, 1984) It is desired to prepare a 25°C aqueous solution of potassium sulfate containing 0.09 g K_2SO_4/g solution in an agitated 48 in. diameter stainless steel reactor. Calculate:

(a) The solid–liquid mass transfer coefficient at N_{js}, the minimum impeller speed required to suspend the potassium particles completely.

(b) The rate of dissolution of the solids at N_{js}.

The required data for solving this problem include:

Solid loading	0.05 g/cm^3 of solid free liquid
Solution viscosity	1.01 cP or 0.00101 kg/m · s
Solution density	1.08 g/cm^3 or 1080 kg/m^3
K_2SO_4 density	2.66 g/cm^3 or 2660 kg/m^3
K_2SO_4 particles size	324 μm or 0.000324 m
Solubility of K_2SO_4	0.12 g/g of solution
Bulk concentration	0.09 g K_2SO_4/g solution
Diffusivity of K_2SO_4 in water	9.9×10^{-6} cm^2/s

SOLUTION: (a) For this simple dissolution a high efficiency impeller will be used (see below for the rationale). From Table 10-3 select an A-310 impeller with diameter, D, equal to the half the vessel diameter, T (i.e., D = T/2, 24 in. or 0.61 m and located at T/4 from the vessel bottom). First, calculate N_{js} using the Zwietering correlation,

$$N_{js} = S\upsilon^{0.1}\left[\frac{g_c(\rho_s - \rho_l)}{\rho_l}\right]^{0.45} X^{0.13} d_p^{0.2} D^{-0.85} \tag{10-25}$$

The value of S from Table 10-3 for a T/2 A-310 located at a clearance of T/4 from the vessel bottom is 7.1.

$$N_{js} = 7.1\left(\frac{0.00101}{1080}\right)^{0.1}\left[\frac{9.81(2.66 - 1.08)}{1.08}\right]^{0.45}\left(\frac{0.09 \times 100}{1 - 0.09}\right)^{0.13} \times (0.000324)^{0.2}(0.61^{-0.85})$$

$$= 2.4 \text{ rps or } 144 \text{ rpm}$$

Second, calculate the Sherwood number, Sh, using the correlation developed by Nienow and Miles (1978):

$$Sh = 2 + 0.44\ Re_p^{1/2} Sc^{0.38} \tag{10-26}$$

The Schmidt and Reynolds numbers for this system are

$$Sc = \frac{1.01 \times 10^{-2}}{1.08 \times 9.9 \times 10^{-6}} = 945$$

Calculate V_t. As pointed out earlier, the calculation is an iterative one since the equation to use depends on the value of Re_p, which in turn depends on V_t. An

equation solver such as TK Solver can be used to quickly perform the required iterative solution. For this system it turns out that the intermediate law is what applies, as shown below. So we use eq. (10-3) and the appropriate expression for C_D from Table 10-1:

$$V_t = \sqrt{\frac{4g_c d_p(\rho_s - \rho_l)}{3C_D\rho_l}} \tag{10-27}$$

where C_D is given by
$C_D = 18.5/Re_p^{3/5}$ and Re_p by

$$Re_p = \frac{\rho_l V_t d_p}{\mu} \tag{10-28}$$

Substituting values in eqs. (10-3) and (10-4), we obtain

$$V_t = \sqrt{\frac{(4 \times 9.81 \times 0.000324)(2.66 - 1.08)}{3 \times 1.08C_D}}$$

$$Re_p = \frac{(1.08 \times 10^3 \text{ kg/m}^3)(V_t \text{ m/s})(0.000324 \text{ m})}{0.00101 \text{ Kg/m} \cdot \text{s}}$$

Solving these iteratively with an equation solver, we obtain

$$V_t = 0.04 \text{ m/s or } 0.13 \text{ ft/sec} \qquad \text{and} \qquad Re_p = 14$$

The value of Re_p is within the intermediate law regime; therefore, we accept the settling velocity calculated.

Substituting the values for Re_p, and Sc into eq. (10-23) gives

$$Sh \equiv \frac{k_{SL}d_p}{D_A} = 2 + 0.44 \times 14^{1/2}(945^{0.38})$$
$$= 24$$

and therefore

$$k_{SL} = Sh\frac{D_A}{d_p} = 24 \times \frac{9.9 \times 10^6}{0.0324}$$
$$= 7.4 \times 10^{-3} \text{ cm/s}$$

(b) The initial dissolution rate corresponds to the case where $[A] = 0$ and can now be calculated with eq. (10-17) as follows.

$$a_p = 6\frac{5 \times 10^{-2}}{2.66 \times 3.24 \times 10^{-2}} = 3.5 \text{ cm}^2/\text{cm}^3$$

The initial rate of dissolution using eq. (10-16) is

$$M = (7.4 \times 10^{-3} \times 10^{-3} \times 3.5)(0.12 \times 1.08 - 0.0)\ \text{g/cm}^3 \cdot \text{s}$$
$$= 3.36 \times 10^{-3}\ \text{g/cm}^3 \cdot \text{s}$$

Note that as the particles dissolve: (1) the particle size, d_p, decreases; (2) the bulk concentration increases, thus decreasing the driving force, and (3) k_{SL} increases. These time-dependent changes have to be accounted for to obtain the final dissolution rate and how long it takes to dissolve all the particles completely.

10-5 SELECTION, SCALE-UP, AND DESIGN ISSUES FOR SOLID–LIQUID MIXING EQUIPMENT

The selection, scale-up, and design of the components that make up the mixing system are based on the fundamental and experimental descriptions of the hydrodynamics and mass transfer aspects of solids suspension discussed earlier. The following issues must be addressed:

1. Process needs assessment, including:
   a. Phases—solid, liquid, and gas—present or occurring during the process
   b. Mixing operations and the desired process results
   c. Unit operations of interest
   d. Quantities and properties of solid and liquid phases
2. Vessel design and internals, including:
   a. Bottom head design
   b. Size and dimensions
   c. Baffles and other internals
3. Selection and design of the agitator or mixer components, including:
   a. Impeller type, number, and dimensions
   b. Impeller location in the vessel
   c. Impeller speed and power
   d. Shaft diameter and length
   e. Drive and seal system

10-5.1 Process Definition

The first task in analyzing a mixing problem, determining experiments to perform for mixer scale-up, or designing a mixing system is to define the process needs. It is important to consider carefully the potential impact of mixing on all the physical and chemical phenomena necessary to achieve the desired process result. Invariably, one of these phenomena will be the critical operation on which to base the selection, scale-up, or design of the mixing system.

The definition should include:

- A list of all the phases of matter (gas, liquid, solid) involved or that can occur, even by accident, from start to end of the process; in particular, instances where two or more phases coexist must be noted.
- A list of all the mixing operations (blending, solids suspension, gas dispersion, immiscible liquids dispersion, etc.) involved in the process or carried out in the same vessel.
- A statement of the purpose and duty of the mixing operations, including the desired process result. For solids suspension, one must choose from among the applicable process objectives as well as the desired degree of suspension. The selection must be based on knowledge of the process determined experimentally or by comparison with a similar process.
- The quantities of solid and liquid phases involved as well as the properties of the solid and liquid to assess how difficult it might be to achieve the aforementioned desired results.

10-5.2 Process Scale-up

Scale-up is an effort to understand the fundamental phenomena occurring in a process in order to predict the performance in larger scale equipment. It begins with process research at the bench scale, often in small glassware, through pilot scale studies to full production. The value of scale-up is captured in the following comment attributed to L. H. Baekland, the father of plastics: "Commit your blunders on a small scale and make your profits on a large scale."

In solid–liquid mixing applications, the purpose of scale-up is to determine the operating conditions at different scales at which mixing yields equivalent process results. The tasks involve:

1. Definition of the appropriate desired process result, such as level of uniformity of the solid distribution in a vessel, the time to achieve complete dissolution, the rate of reaction between a solid and a liquid reactant, and so on.
2. Developing reliable correlations that describe the effects of key process properties, mixer design, and operating variables on the desired process result by either experimentation or mathematical analysis of the physicochemical phenomena
3. Determining and confirming the key controlling physicochemical phenomena and the associated correlating parameters, preferably in dimensionless form
4. Applying the key correlations to predict the process performance at different scales

Occasionally, heuristics based on extensive experience with similar processes are sufficient. Often, especially for processes involving multiple phases or fast

reactions, it is necessary to perform several experiments at two or more different scales, where the vessel size based on diameter is varied by at least a factor of 2.

10-5.3 Laboratory or Pilot Plant Experiments

Simple laboratory or pilot plant experiments carried out in transparent vessels, such as glassware, where one can observe the behavior of the various phases during agitation often provides great insight and understanding of the mixing challenges and opportunities. Often, these are augmented with pilot scale tests to determine or evaluate pertinent scale-up requirements. The lab experiments should be designed to answer specific process-related questions such as those discussed. Ultimately, the tests should provide information including:

1. The desired level of suspension required by the process
2. The properties of the solids and liquids required to estimate the necessary solid–liquid mixing parameters, including:
   a. Settling velocity, V_t
   b. Minimum speed for suspension, N_{js}
   c. Solid–liquid mass transfer coefficient, k_{SL}
   d. Materials of construction

In the various correlations presented earlier, the magnitude and sign of the exponents on the variables establish their parametric effects and may be used as a guide for selection of the more sensitive parameters to explore in a laboratory or pilot plant.

Typical lab experiments must include evaluation of the following effects:

1. Impeller speed to establish the effect, if any, on the process result as well as the speed beyond which there is no further significant gain in or deterioration of the desired process results
2. Particle size to determine the effect on reaction rates for solid-catalyzed reactions: in particular, the particle size at which mass transfer effects are negligible
3. Addition rate of solids and/or liquid, as well as the ratio of solids to liquid to determine their effects on rheology, suspension level, reaction, or other mass transfer rate
4. Impeller design and geometry to explore the relative effects of flow and shear distribution in the vessel for particle size control, micromixing for fast kinetics, and so on. Geometric ratios of importance include:
   a. Ratio of the impeller to tank diameter, D/T, to determine the effect of the ratio of overall pumping capacity to fluid shear
   b. Blade width to impeller diameter, W/D, to evaluate the relative effects of microscale and macroscale mixing processes and also fluid shear rates

5. Number and location of the impeller to explore the effect of liquid coverage on headspace gas entrainment, uniformity of solids distribution, and so on. Parameters of interest include:
   a. Ratio of the impeller clearance from vessel bottom to tank diameter, C/T
   b. Ratio of liquid coverage above impeller to tank diameter, CV/T
6. Baffle design and location to explore effects of vortex formation for entrainment of floating solids, and so on.

10-5.4 Tips for Laboratory or Pilot Plant Experimentation

In any laboratory or pilot plant tests, the first thing to vary is the impeller speed. This changes pumping capacity, blend time, and shear rates.

- On-bottom motion or partial suspension is rarely a useful desired mixing result except, perhaps, for the dissolution of very soluble solids.
- Complete suspension is the minimum desired mixing goal for most solid–liquid mixing operations involving settling solids. The equivalent condition for floating solids is complete incorporation and dispersion of the floating solids.
- Uniform suspension is required for crystallization, solid-catalyzed reactions, and suspension polymerization where high local concentrations may lead to poor yields of the desired product. Also, as practical as possible, crystallization slurries must be fed to a centrifuge at a uniform solids concentration for the proper cake buildup required for effective filtration and washing of the solid cake.
- Specified mass transfer rate such as dissolution rate, reaction rate, and so on, may be the desired process result to achieve a given production capacity.
- Particle size control may be the desired result in certain formulation operations.
- The measurement of power on a full or pilot scale vessel is best accomplished with a wattmeter. Ammeter readings, at best, must be ratioed to the full-load nameplate amperage, which varies with voltage, power factor, and motor type.
- For the fractional-horsepower motor used in the laboratory or pilot plant, power draw is best determined by calculation using the defining equation for the power number. This requires power number versus Reynolds number data or correlation.
- To estimate the viscosity of complex non-Newtonian slurries, Oldshue and Sprague (1974) recommend the use of a mixing viscometer that mimics the hydrodynamic environment likely to be encountered in an agitated vessel.

10-5.5 Recommendations for Solid–Liquid Mixing Equipment

Solids suspension is usually carried out in mechanically agitated vessels with or without draft tubes. A schematic representation of a typical mechanically agitated vessel is shown in Figure 10-7. A mechanically agitated vessel with a draft tube employed for certain crystallization operations is shown in Figure 10-8.

In the following sections we provide several design guidelines and examples of the selection, design, and operation of equipment for solid–liquid mixing.

10-5.5.1 Vessel Geometry and Vessel Nozzles. The vessel design, in particular, the bottom head design, can have a profound effect on the agitation requirements for a given desired result. The bottom head geometry influences the flow patterns responsible for lifting solids up from the vessel bottom.

Design Tip. Dished heads (ASME dished, elliptical, or torispherical heads) are the preferred design. To achieve complete suspensions, flat-bottomed heads require 10 to 20% higher impeller speeds than for dished heads (Mak, 1992). Conical bottoms must be avoided.

The aspect ratio of the vessel—actually, the ratio of liquid depth, H, to vessel diameter, T (see Figures 10-7 and 10-8)—is an important determinant of the number of impellers to be used. The fluid velocities decrease with increasing distance from the impeller region and may not be sufficient to counteract the tendency of the solid to settle. Also, impellers mounted far above the vessel base

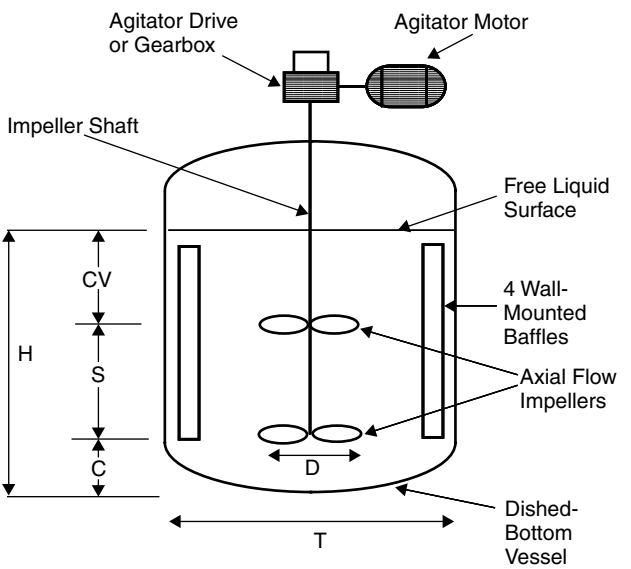

Figure 10-7 Schematic representation of a typical mechanically agitated vessel.

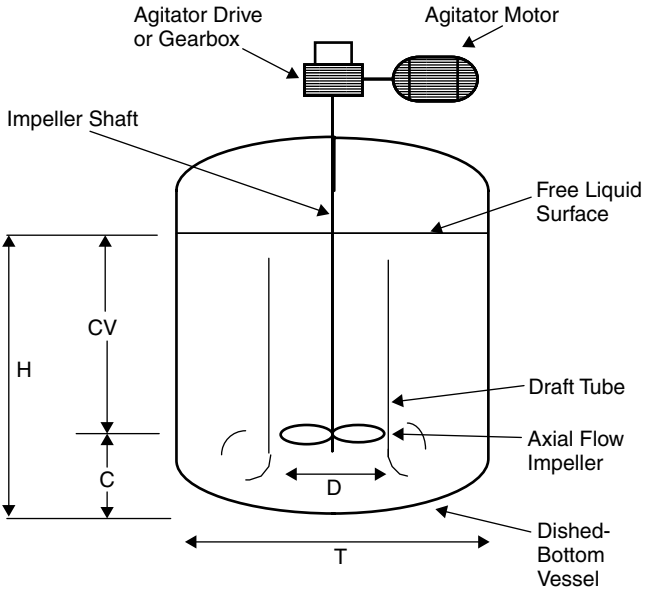

Figure 10-8 Mechanically agitated vessel with a draft tube.

may not generate enough turbulent velocity at the base of the vessel to lift any settled solids.

Design Tips

- A single impeller is usually sufficient for off-bottom suspension in vessels with dished heads, $H/T < 1.3$.
- Dual impellers are recommended for vessels with $1.3 < H/T < 2.5$, used for uniform suspension of fast-settling solids.
- Three impellers may be required if $2.5 < H/T$. A vessel with such a high aspect ratio is a poor choice for solid suspension.
- Vessel nozzles should be located and oriented to avoid or minimize any interference with the mixing system's performance.

Nozzle Design Tips

- Nozzles and dip pipes for liquid addition should not allow the liquid jet to impinge directly on the impeller. At too high a liquid jet velocity, the jet force will contribute to higher shaft deflections.
- Dip pipes and other probes must be supported—usually by attaching to wall-mounted baffles—or stiff enough to withstand the bending moments imposed by the fluid forces. Discuss with your local mechanical engineer.

- Install grating or screen on nozzles for solid addition to keep very large solid chunks or foreign matter from the liquid.
- Bottom nozzles should be as short as practical and be installed with flush-bottom valves to prevent solids from collecting.

10-5.6 Baffles

Baffles are highly recommended for solids suspension operations involving solids that are heavier than the liquid. They convert the swirling motion into top-down or axial fluid motion that helps to lift and suspend the solids (see Visual Mixing CD for an illustrative video). For floating solids, consider the use of submerged or partial baffles to achieve a controlled vortex to draw down the floating solids as recommended by Joosten et al. (1977), Hemrajani et al. (1988), Thring (1990), and Siddiqui (1993).

Baffle Design and Installation Tips

- In steel or alloy vessels, the recommended baffle design for solid suspension of settling solids is four flat blade baffles, each with width, B, equal to T/12 at a wall clearance of at least T/72. The baffles should extend to the lower edge of the lower impeller or to the lower tangent line.
- In glass-lined equipment, the recommended baffles are either fin or beaver-tail type (see Chapter 17). A minimum of two baffles is recommended. These baffles are generally less effective than the standard four flat blade baffles.
- Fin baffles must be installed with the edge of the fin pointing toward the vessel wall; the flat face must be perpendicular to the tangential flow.

10-5.7 Selection and Design of Impeller

Solids suspension and solids distribution is governed primarily by the bulk or convective flows in a vessel. *High efficiency impellers* (e.g., Lightnin A310 and A320, Chemineer HE3, APV LE20, Ekato Viscoprop), whose discharge is flow dominated as well as axially directed, are more efficient than others in achieving solids suspension. However, high efficiency impellers may be a poor choice when the solid suspension is accompanied by other mixing duties, such as liquid–liquid dispersion or gas dispersion. For these cases a multiple-impeller system consisting of a high efficiency impeller in combination with a 45° pitched blade impeller should be evaluated in pilot plant studies.

Small pitched blade impellers with diameter $D < T/2.5$, located nearer the vessel base ($C < T/4$), are good for solid suspension (see Table 10-3). They also aid in the discharge of the solids during slurry transfer. Typical values for impeller clearance are T/4 for hydrofoils and T/3 for pitched blade turbines.

For glass-lined vessels, one is no longer limited to the Pfaudler "crowfoot," also known as the *retreat blade* or *retreat curve impeller* (RCI). Most impeller

designs can now be obtained with a glass lining. Removable glassed impeller designs are preferred over the integral glassed shaft-impeller design (see Chapters 6 and 17).

10-5.8 Impeller Speed and Power

The impeller speed recommended will in general be higher than N_{js}, the speed required for the just suspended state estimated by the Zwietering correlation. The speed required should be based on experimental data. For quick estimates of the speed and power requirements for complete uniformity, the ratios in Table 10-2 may be applied to the estimated value of N_{js}.

Design Tip. For multiprocess batch reactors, mixers equipped with variable speed drives permit the mixer to be operated at different impeller speeds to accommodate the different mixing needs of the various steps in the process.

10-5.9 Shaft, Hub, and Drive

In the design of the shaft and drive system (see Chapter 21), careful consideration should be given to issues, including the need for:

- Startup of the mixer in settled solids.
- Filling and emptying while the mixer is running—the fluid forces on the impeller and shaft are amplified significantly when the liquid surface runs through the impeller, causing severe shaft deflections and vibrations.
- Ensuring that the suspension is maintained during emptying of the vessel to very low levels—for top-mounted agitators, a longer shaft fitted with a smaller-diameter impeller; a tickler, located at the lowest possible clearance from the base of the vessel, is required.
- Employing the same mixer for multiple mixing operations in the same process or for different processes.

Design Tip. The need for startup of a mixer in settled solids will require a larger shaft. This should be stated clearly in any mixer specification or request for quotation. The American Gear Manufacturing Association (AGMA) service rating for the gearbox will be higher. The shaft and gearbox design should be based on a minimum service rating factor of 2. An experienced mechanical engineer should be consulted for help in specifying the mixer or in reviewing any vendor proposals or quotations.

Mixing equipment suppliers have calculational tools to size the shaft to minimize shaft deflections.

Design Tip. Sizing mixers to handle startup in settled solids requires measuring torque under test conditions with actual settled solids. In the absence of such a measurement, any design for such conditions can only be a "wild" guess. Use

other means, such as air sparging, lancing with high-pressure liquid, heating to melt or dissolve the solid, and so on, to loosen the settled solid first. Before attempting to start the agitator drive, check and confirm by hand-turning the shaft that the impeller is indeed free.

NOMENCLATURE

Dimensional Variables and Parameters

a_p	interfacial area for mass transfer per volume of fluid (ft^2/ft^3, m^2/m^3)
$[A^*]-[A]$	concentration driving force (mol/ft^3, mol/m^3)
C	impeller clearance from the bottom of the vessel (ft, m)
CH	cloud height (−)
CV	liquid coverage above the impeller (ft, m)
D	Impeller diameter (ft, m)
D_A	diffusivity (ft^2/h, m^2/s)
$(d_p)_{43}$	mass-mean diameter (ft, m)
d_i	mean particle diameter of the ith size (ft, m)
d_p	particle size or diameter (ft, or m)
g_c	gravitational constant (32.17 ft/sec^2 or 9.81 m/sec^2)
k_{SL}	diffusional mass transfer coefficient
M	rate of diffusional mass transfer
N	impeller speed (rps)
n_i	number of particles in the ith size class
N_{js}	impeller speed for "just suspended" state of particles (rps)
P	impeller power (hp, W)
T	vessel diameter (ft, m)
V_t	particle-free settling velocity (ft/s, or m/s)
V_{ts}	particle-hindered settling velocity (ft/s, or m/s)
X	mass ratio of suspended solids to liquid time 100 (kg solid/kg liquid)×100
Z	liquid depth in vessel (ft, m)

Dimensionless Parameters

C_D	drag coefficient
$Fr = \left(\frac{\rho_l}{\rho_s - \rho_l}\right) N_{ts}^2 D/g_c$	Froude number
N_{Fr}	Froude number
N_p	impeller power number
Re_p	particle Reynolds number
$Re_{imp} = N_{js}D^2/\nu$	impeller Reynolds number

S	Zwietering constant, dimensionless number which is a function of impeller type, as well as D/T, C/T
Sc	Schmidt number
Sh	Sherwood number

Greek Symbols

μ_l	liquid viscosity (cP or Pa · s)
ν	kinematic viscosity of the liquid (m^2/sec)
ρ_l	liquid density (lb/ft^3 or kg/m^3)
ρ_s	solid or particle density (lb/ft^3, kg/m^3)
ϕ	volume fraction of solid
ϕ	solid loading (g/cm^3 solid-free liquid)
ψ	particle shape or sphericity, (dimensionless factor defined by the ratio of surface area of a spherical particle of the same volume to that of a nonspherical particle)
χ	volume fraction of solids in suspension

REFERENCES

Armenante, P. M., and E. U. Nagamine (1998). Effect of low off-bottom impeller clearance on minimum agitation speed for complete suspension of solids in stirred tanks, *Chem. Eng. Sci.*, **53**(9), 1757–1775.

Armenante, P. M., E. U. Nagamine, and J. Susanto (1998). Determination of correlations to predict the minimum agitation speed for complete solid suspension in agitated vessels, *Can. J. Chem. Eng.*, **76**, 413–419.

Bakker, A., J. B. Fasano, and K. J. Myers (1994). Effect of flow pattern on solids distribution in a stirred tank, *Inst. Chem. Eng. Symp. Ser.*, **136**, 65–72.

Baldi, G., R. Conti, and E. Alaria (1978). Complete suspension of particles in mechanically agitated vessels, *Chem. Eng. Sci.*, **33**, 21.

Becker, H. A. (1959). The effects of shape and Reynolds number on drag in the motion of a freely oriented body in an infinite fluid, *Can. J. Chem. Eng.*, **37**, 85–91.

Bittorf, K. J., and S. M. Kresta (2002). Prediction of cloud height for solid suspension in stirred tanks, *CHISA Conference Proc.*, Prague, Aug. 25–29.

Bujalski, W. K., et al. (1999). Suspension and liquid homogenisation in high solids concentration stirred chemical reactors, *Trans. Inst. Chem. Eng.*, **77**, 241–247.

Chapman, C. M. (1981). Studies of gas–liquid–particle mixing in stirred vessels, Ph.D. dissertation, University of London.

Chapman, C. M., A. W. Nienow, and M. Cooke (1983). Particle–gas–liquid mixing in stirred vessels: 1. Particle–liquid mixing, *Chem. Eng. Res. Dev.*, **61**, 71–81.

Chaudhari, R. V. (1980). Three phase slurry reactors, *AIChE J.*, **26**, 179.

Choudhury, N. H. (1997). Improved predictive methods for solids suspension in agitated vessels at high solids loadings, Ph.D. dissertation, University of Arkansas, Fayetteville, AR.

Choudhury, N. H., W. R. Penney, K. Meyers, and J. B. Fasano (1995). An experimental investigation of solids suspension at high solids loadings in mechanically agitated vessels, *AIChE Symp. Ser.*, **305**(91), 131–138.

Cleaver, J. W., and B. Yates (1973). Mechanism of detachment of colloidal particles from a flat substrate in turbulent flow, *J. Colloid Interface Sci.*, **44**, 464.

Conti, R., and S. Sicardi (1982). Mass transfer from freely-suspended particles in stirred tanks, *Chem. Eng. Commun.*, **14**, 91.

Davis, R. H., and H. Gecol (1994). Hindered settling functions with no empirical parameters for polydisperse suspensions, *AIChE J.*, **40**, 570–575.

Doraiswamy, L. K., and M. M. Sharma (1984). *Heterogeneous Reactions: Analysis, Examples and Reactor Design*, Vol. 2, *Fluid–Fluid–Solid Reactions*, Wiley, New York, pp. 233–316.

Froment, G. F., and K. B. Bischoff (1990). *Chemical Reactor Analysis*, Wiley, New York.

Guerci, D., R. Conti, and S. Sicardi (1986). *Proc. International Colloquium on Mechanical Agitation,* ENSIGC, Toulouse, France, pp. 3–8 to 3–24.

Guiraud, P., J. Costes, and J. Bertrand (1997). Local measurements of fluid and particle velocities in a stirred suspension, *Chem. Eng. J.*, **68**, 75–86.

Hemrajani, R. R., et al. (1988). Suspending floating solids in stirred tanks: mixer design, scale-up and optimization, *Proc. 6th European Conference on Mixing*, Pavia Italy, May 24–26, pp. 259–265.

Hicks M. T., et al. (1993). Cloud height, fillet volume, and the effect of multiple impellers in solid suspension, presented at Mixing XIV, Santa Barbara, CA, June 20–25.

Hicks M. T., K. J. Myers, and A. Bakker (1997). Cloud height in solids suspension agitation, *Chem. Eng. Commun*., **160**, 137–155.

Ibrahim, S. B., and A. W. Nienow (1994). The effect of viscosity on mixing pattern and solid suspension in stirred vessels, *Inst. Chem. Eng. Symp. Ser*., **136**, 25–36.

Joosten, G. E. H., J. G. M. Schilder, and A. M. Broere (1977). The suspension of floating solids in stirred vessels, *Trans. Inst. Chem. Eng.*, **55**, 220.

Levins, D. M., and J. Glastonbury (1972a). Application of Kolmogoroff's theory to particle–liquid mass transfer in agitated vessels, *Chem. Eng. Sci*., **27**, 537–542.

Levins, D. M., and J. Glastonbury (1972a). Particle–liquid hydrodynamics and mass transfer in a stirred vessel, *Trans. Inst. Chem Eng*., **50**, 132–146.

Mak, A. T. C. (1992). Solid–liquid mixing in a mechanically agitated vessel, Ph.D. dissertation, University College–London.

Maude (1958). Cited in *Chemical Engineers' Handbook*, R. H. Perry and D. Green, eds., McGraw-Hill, New York, 1984, pp. 5–66.

Mullins, J. W. (1993). *Crystallization*, 3rd ed., Butterworth, London.

Nienow, A. W. (1968). Suspension of solid particles in turbine-agitated baffled vessels, *Chem. Eng. Sci.*, **23**, 1453.

Nienow, A. W. (1975). Agitated vessel particle–liquid mass transfer: a comparison between theories and data, *Chem. Eng. J.*, **9**, 153.

Nienow, A. W. (1985). The dispersion of solids in liquids, in *Mixing of Liquids by Mechanical Agitation*, J. J. Ulbrecht and G. K. Patterson, eds., Gordon & Breach, New York, pp. 273–307.

Nienow, A. W., and D. Miles (1978). The effect of impeller/tank configurations on fluid–particle mass transfer, *Chem. Eng. J.*, **15**, 13.

Oldshue, J. Y. (1983). Fluid mixing technology and practice, *Chem. Eng.*, June 13, pp. 83–108.

Oldshue, J. Y., and J. Sprague (1974). Theory of mixing, *Paint Varnish Prod.*, **3**, 19–28.

Parfitt, G. D. (1973). *Dispersion of Powders in Liquids*, 2nd ed., Applied Science Publishers, London.

Perry, R. H., and D. Green (1984). In *Chemical Engineers' Handbook*, R. H. Perry and D. Green, eds., McGraw-Hill, New York, pp. 5–63, 5–68.

Pettersson, M., and A. C. Rasmuson (1998). Hydrodynamics of suspensions agitated by a pitched-blade turbine, *AIChE J.*, **44**(3), 513–527.

Pettyjohn (1948). Cited in *Chemical Engineers' Handbook*, R. H. Perry and D. Green, eds., McGraw-Hill, New York, 1984, pp. 5–64.

Rao, K. S. M. S. R., V. B. Rewatkar, and J. B. Joshi (1988). Critical impeller speed for solid suspension in mechanically agitated contactors, *AIChE J.*, **34**(8), 1332.

Rieger, F., and P. Ditl (1994). Suspension of Solid Particles, *Chem. Eng. Sci.*, **49**(14), 2219–2227.

Shamlou, P. A., and A. Zolfagharian (1990). Suspension of solids in liquid-jet stirred vessels, *Fluid Mixing IV*, H. Benkreira, ed., Hemisphere Publishing, Washington, DC, pp. 365–377.

Siddiqui, H. (1993). Mixing technology for buoyant solids in a non-standard vessel, *AIChE J.*, **39**(3), 505.

Thring, R. W. (1990). An experimental investigation into the complete suspension of floating particles, *Ind. Eng. Chem.*, **29**, 676.

Zolfagharian, A. (1990). Solid suspension in rotary-stirred and in liquid-jet stirred vessels, Ph.D. dissertation, University College–London.

Zwietering, T. N. (1958). Suspending of solid particles in liquid by agitators, *Chem. Eng. Sci.*, **8**, 244.